Suppression of purely elastic instabilities in the torsional flow of viscoelastic fluid past a soft solid

R. Neelamegam, V. Shankar, and Debopam Das

Citation: Phys. Fluids **25**, 124102 (2013); doi: 10.1063/1.4840195
View online: http://dx.doi.org/10.1063/1.4840195
View Table of Contents: http://pof.aip.org/resource/1/PHFLE6/v25/i12
Published by the AIP Publishing LLC.

PHYSICS OF FLUIDS **25**, 124102 (2013)

Suppression of purely elastic instabilities in the torsional flow of viscoelastic fluid past a soft solid

R. Neelamegam,[1] V. Shankar,[1,a)] and Debopam Das[2]
[1]*Department of Chemical Engineering, Indian Institute of Technology, Kanpur 208016, India*
[2]*Department of Aerospace Engineering, Indian Institute of Technology, Kanpur 208016, India*

(Received 2 March 2013; accepted 21 November 2013; published online 13 December 2013)

Experiments are performed to explore the role of a soft, deformable solid layer on the purely elastic instability in the torsional flow of polymer solutions between two circular discs. The gel layer is placed on the stationary bottom plate of a rheometer, and the polymer solution is placed between the gel and the rotating top disc. The observed variation of viscosity with shear rate (or shear stress) is correlated with the presence or absence of purely elastic instability in the viscometric flow. Earlier work has shown that with increase in shear rate, the torsional flow of a polymer solution between rigid discs undergoes transition from the simple viscometric flow state to elastic turbulence via a sequence of instability modes. We combine rheological observations and flow visualization to show that the deformable solid has a profound effect on the stability of the torsional flow. In marked contrast to flow between rigid plates (where the fluid shows apparent shear-thickening at the onset of instability), the apparent viscosity continues to decrease up to a much larger value of shear rate with the presence of a soft gel. At a fixed shear rate, for flow past a soft gel, the measured stress does not exhibit marked temporal fluctuations that would otherwise be present without the soft gel. Using flow visualization, we show that secondary flow patterns that form after the instability for a rigid surface disappear for flow on soft gel surfaces. In the case of rigid surfaces, the instability is sub-critical and exhibits hysteresis behavior, which again is absent when the flow occurs past a soft solid layer. Our results show that the role of the soft deformable solid is to suppress the purely elastic instability in torsional flows of polymeric liquids for intermediate shear rates. While it is known that soft deformable solids destabilize the flow of Newtonian liquids in the absence of inertial effects, our study shows that the effect of deformability can be opposite in the torsional flow of viscoelastic liquids.
 [http://dx.doi.org/10.1063/1.4840195]

I. INTRODUCTION

Torsional flows of viscoelastic polymer solutions are well-known to undergo a transition from viscometric (laminar) to a much more complex and apparently turbulent regime through a sequence of instability patterns even at very low Reynolds number.[1–10] Such instabilities at negligible fluid inertia are driven by elastic forces in the polymer solution, and are often referred to as "purely elastic" instabilities.[7] With increase in the shear rate (or angular velocity), different instability patterns form sequentially. Each instability pattern is characterized by unique structural and rheological characteristics. In this paper, we carry out experiments on torsional flow of viscoelastic polymer (polyacrylamide) solutions over soft solid materials, in order to examine the role of the solid layer deformability on the purely elastic instability. The motivation for studying this configuration is two-fold: First, in many microfluidic applications, soft elastomers are used for fabricating sub-millimeter scale[11,12] channels, and often the fluid is a polymer solution (e.g., a solution containing DNA

a)Author to whom correspondence should be addressed. Electronic mail: vshankar@iitk.ac.in

molecules). It is of interest in such applications to understand the fundamental nature of flow of a polymer solution past a deformable solid material. For instance, if instabilities in flow of polymer solutions can be initiated by the deformability of the solid, this could be potentially exploited in improving mixing in such microfluidic devices. Second, in a completely different context, there is a lot of current interest in the dynamics of flow of worm-like micellar solutions[13–15] which exhibit shear-banding that leads to the co-existence of a gel-like phase and a fluid-like phase. This closely resembles the configuration explored in this paper, and the experiments carried out in this paper would serve to further the fundamental understanding of dynamics of such shear-banded states. In the remaining part of this Introduction, we review the relevant literature and motivate the context for this study.

The purely elastic instability was first studied theoretically by Phan-Thien,[1] for torsional flow between parallel plates using the Oldroyd-B model. He predicted that the instability appears when $\lambda\Omega > \pi/\sqrt{\beta(2\beta+3)}$, where λ is the relaxation time, Ω is the angular speed of rotating plate, and $\beta = \eta_p/\eta$ is the ratio of polymer contribution to the viscosity (η_p) to the total viscosity η of the solution. Subsequently, torsional flow in the cone-and-plate geometry was studied by Phan-Thien[2] using Oldroyd-B model, and he predicted that a similar instability appears when $\lambda\Omega > \pi\sqrt{2/(5\beta)}$. Olagunju and Cook[5] carried out an asymptotic analysis for small cone angles α, and obtained solutions for the steady axisymmetric flows in the cone-and-plate configuration. Their results are in qualitative agreement with those of Phan-Thien,[2] but they pointed out some corrections in the expression for the critical Deborah number expression reported in Ref. 2. Magda and Larson[3] carried out experiments to study the instability using polyisobutylene and polystyrene Boger fluids with parallel plate and cone-and-plate arrangements. They observed that the critical shear rate for instability is inversely proportional to the fluid thickness between the plates (for parallel-plate configuration) and cone angle (for cone-and-plate configuration). The purely elastic instability has been studied with a focus on the effect of fluid thickness and cone angle using polyisobutylene Boger fluids by McKinley *et al.*[4] They observed that both shear stress and first normal stress difference showed large temporal fluctuations for a fixed Deborah number, in case of both cone-and-plate and parallel-plate arrangements. They further carried out experiments to demonstrate hysteresis in the flow by observing the apparent shear stress in the solution at different shear rates. After a critical shear rate, the shear stress shows a rapid increase to a new value (very different from the shear stress appropriate to the basic viscometric flow). Further increase in shear rate resulted in a new flow state with difference in the apparent shear stress to the base flow shear stress increasing with the shear rate. When the shear rate was decreased, the flow state suddenly jumps to the base flow state, without fully retracing the path followed during increase of shear rate. This is indicative of strong hysteresis in the flow and suggests that the instability is sub-critical in nature with multiple shear stress values existing for a given shear rate.

The experimental results are often represented in terms of either a Deborah number ($De \equiv \Omega\lambda$) or a Weissenberg number ($Wi \equiv \dot{\gamma}\lambda = \lambda\Omega R/d$), where $\dot{\gamma}$ is the shear rate, R is the radius of the disc, and d is the fluid thickness. All previous experiments show that the shear rate required for instability is inversely proportional to d, and this can be represented in dimensionless terms as either the De required for instability being independent of thickness, or the Wi for instability being proportional to R/d. Using flow visualization, McKinley *et al.*[4] observed both axisymmetric and non-axisymmetric (time-dependent) secondary flow structures. Byars *et al.*[6] studied the elastic instability using polyisobutylene solution flow in the parallel-plate arrangement. They observed a sequence of instability modes (both axisymmetric and non-axisymmetric) depending on fluid characteristics and thickness of fluid. They also visualized the flow patterns, and determined the wave speed and wave dimensions. In addition, linear stability analysis was carried out using the Chilcott-Rallison constitutive equation which agreed with the experimental observations.

Groisman and Steinberg[8] first observed the "elastic turbulent" state at negligible fluid inertia using viscous polyacrylamide solutions in the parallel plate arrangement. Since much larger aspect ratios ($d/R = 0.263$ and 0.526) were used in the experiment, this resulted in direct transition from base flow to the elastic turbulence. The resistance offered by the flow due to the turbulence was found to be 20-fold higher compared to the laminar flow. Imaging of the secondary flow patterns (elastic turbulence) and Doppler velocity measurement revealed a power-law decay of velocity

fluctuations with frequency. It was noted that the shape of flow pattern is a "toroidal vortex." Recently, Schiamberg *et al.*[10] experimentally studied the transitional pathway from the viscometric laminar flow to elastic turbulence using a 492 ppm polyacrylamide solution ($M_w = 18 \times 10^6$ g mol^{-1}) in parallel plate arrangement. The transition was observed to be accompanied by different modes of instability such as the stationary ring, competing spiral, multispiral-chaotic, and spiral bursting modes. Flow visualization, time-dependent stress variation, and analysis of secondary flows were used for differentiating the various instability modes. Low molecular weight ($M_w \sim 5 \times 10^6$ g mol^{-1}) polyacrylamide solution with varying concentrations (200, 400, and 800 ppm) were further used for understanding the universal features of the transition. The higher concentration solution (800 ppm) exhibited an oscillatory instability mode with definite frequency, which was not observed for lower concentrations.

Previous studies have also investigated the effect of soft gels on the stability of torsional Couette flow of Newtonian fluids using the parallel-plate arrangement of a rheometer. Kumaran and Muralikrishnan[16,17] coated the bottom plate of the rheometer (in the parallel-plate configuration) with a soft gel, and studied the effect of the gel on the flow of (Newtonian) silicone oil. They found that for small shear rates, the viscosity of the silicone oil agrees with its reported value. However, at larger shear rates, the apparent viscosity deviates from the reported value, as the flow between the top plate and the gel is no longer viscometric due to the instability of the interface between the liquid and the gel. They used the dimensionless parameter $\Gamma = (\dot{\gamma}\eta/G')$, which is the ratio of viscous forces in the liquid to elastic forces in the solid, to characterize the instability. Here, $\dot{\gamma}$ is the shear rate in the fluid, η is the viscosity of the fluid, and G' is the shear modulus of the solid. Beyond a critical value of Γ, the flow becomes unstable for fixed value of ratio of thickness of gel (H) and fluid (d), and gel-to-fluid viscosity ratio (η_g/η). The value of Γ at which the flow becomes unstable agreed well with the theoretical predictions,[18] which yield the critical value of Γ (the minimum value in the Γ vs wavenumber curve). Eggert and Kumar[19] experimentally probed the nonlinear dynamics of flow of polypropylene oxide on polydimethylsiloxane gel, after the onset of instability. They observed hysteresis when stress was varied above and below the critical stress, indicative of the subcritical nature of the instability. Experiments have also shown the presence of similar instabilities in the flow of Newtonian fluids through gel-coated tubes.[20]

There have also been few papers[13–15] which experimentally study the dynamics of the shear-banded state in worm-like micellar solutions. These studies show that the shear-banded state comprises of co-existing fluid and gel-like phases. Vasudevan *et al.*[13] observe that upon increase in shear stress, the interface between the gel-like phase and the fluid phase becomes unstable, and they conclude that this is similar to the instability of the interface between the gel and a Newtonian fluid.[17,19] Similar co-existence of gel-like and fluid phases was also reported in Refs. 14 and 15. The configuration explored in the present work mimics the co-existing fluid and gel phases in the shear-banded state, and an explicit investigation of the dynamics of the polymer solution-gel interface will help to better understand the dynamics of the shear-banded state.

In the present study, we carry out experiments to analyze the flow of a viscoelastic polymer solution over soft materials to understand the role of the deformability of the soft solid on the elastic instability driven by normal stress difference. Previous theoretical studies[21,22] have shown that the addition of polymer to a Newtonian fluid results in stabilization of the interfacial instability between the fluid and the gel. However, those theoretical studies were restricted to planar flows, where the purely elastic instability due to curvature of streamlines is absent. For the configuration explored in this paper, which involves the torsional flow of a polymeric liquid past a gel, both the purely elastic instability of the bulk polymer flow, and the flow-induced interfacial instability of the liquid-gel interface can potentially destabilize the system. Will the presence of the soft solid always lead to instability? We address this question by systematically investigating the role of solid layer deformability on the purely elastic instability in a torsional flow of a polymer solution. Remarkably, we find that the flow of polyacrylamide solution over the gel surface exhibits evidence for suppression of the purely elastic instability. By carrying out control experiments on a relatively harder gel, we demonstrate that the suppression of purely elastic instability is indeed due to solid layer deformability. Flow visualization is also carried out to supplement the rheological observations. The rest of the article is structured as follows: In Sec. II, we describe the experimental procedure adopted, including

the details of preparation of the polymeric liquid and soft solid. This is followed by a discussion on the effect of a soft solid layer on the instability in Sec. III A. In the Appendix, we characterize the nature of flow and instability in torsional flow between two rigid circular discs. In Sec. III B, we discuss results from the time-variation of stress at a fixed steady state both in the presence and absence of the soft solid. In Sec. III C, we briefly discuss results obtained from visualizing the flow. Section IV provides a discussion on the plausible mechanism behind the instability suppression in flow past soft gels. Finally, we provide the salient conclusions of this work in Sec. V.

II. EXPERIMENTAL METHODS AND PROCEDURE

The AR 1000N rheometer (TA Instruments, UK) is used in our experiments for studying the flow of viscoelastic polymer solutions over soft materials. The flow occurs (schematic shown in Figure 1) between the rheometer's stationary bottom plate and the rotating top plate. The gap d between the two plates is maintained at 1 mm unless mentioned otherwise. The radius (R) of the top plate of the rheometer is 20 mm and hence the aspect ratio $d/R = 0.05$ in most of our experiments. The polymer solution is placed between the two plates without air entrapment, and the excess solution beyond the top plate is removed carefully. The temperature of the polymer solution is allowed to settle to the ambient temperature ($25 \pm 2\,^{\circ}$C). The rheometer is operated either in the shear rate-controlled or the stress-controlled mode. In the shear rate-controlled mode, the angular velocity (rad/s) Ω (measured at the outer rim) of the top rotating plate is maintained at a steady value. The shear rate is computed as $\dot{\gamma} = R\Omega/d$. In the stress-controlled mode, the torque of the rotating top plate is maintained at a constant value, and the shear stress (τ) is computed as $\tau = 2M/\pi R^3$, where M is the applied torque. This relation is strictly valid for viscometric flow of a Newtonian fluid. When the flow is viscometric, the shear rate is related to the shear stress as $\tau = \eta\dot{\gamma}$. For a constant shear rate, the shear stress is measured and the above equation is used to calculate the apparent viscosity of the fluid. When secondary flow develops at the onset of the instability, the flow in the rheometer is

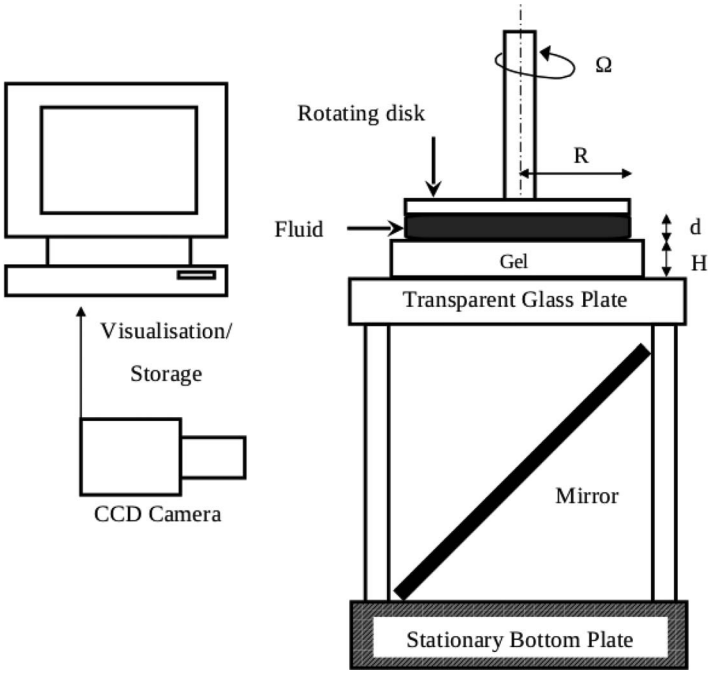

FIG. 1. Schematic diagram of the experimental setup: the standard configuration of the rheometer is modified for polymer solution (present between rotating top disc and the gel) flow past a soft solid layer. The radius R of the rotating top plate is 20 mm. The fluid thickness is d, and the gel thickness is H. The transparent top and side glass plates allow for (diffuse) illumination of the fluid from the bottom. The flow structure is captured using a camera through a 45 $^{\circ}$ mirror placed below the transparent glass plate. The lower side of the top rotating disc is colored in black to aid visualization.

not viscometric, and the viscosity that is computed by the instrument is no longer a material property of the fluid. Instead, it is a measure of the amount of stress in the polymer solution. Indeed, as shown in the earlier studies,[10] the apparent viscosity increases sharply when the flow is not viscometric, and the corresponding shear rate is taken as the critical shear rate at which the viscometric flow becomes unstable. The deviation of the apparent viscosity from its expected value is also used as a signature of instability in the earlier papers that studied the effect of a soft solid on the flow of a Newtonian fluid.[17,19]

In order to carry out experiments at higher aspect ratios ($d/R > 0.075$) in the parallel-plate flow arrangement, we use a petri dish (45 mm diameter; Borosilicate glass—Agarwal) instead of the bottom rigid surface of the rheometer. This petri dish is glued strongly to the bottom plate of the rheometer to avoid movements in any direction. Care is taken to ensure that the petri dish and the top plate are aligned properly. Deceleration arrangement of the top plate is used for zero gap adjustment on the upper surface of the petri dish. The top plate is then raised to the pre-set value of fluid thickness and the polymer solution is carefully loaded.

To study the flow of viscoelastic fluid over soft materials like polymer gels, the standard configuration of the rheometer is modified (following Refs. 17 and 19; Figure 1) as follows. The normal force measuring arrangement at the bottom plate is used for zero gap adjustment. The gel is placed on the bottom plate and normal force is set to zero. The top plate is brought nearer to the gel surface until the normal force sensor senses 0.45 N, and the thickness of the gel (H) is noted at this position. The top plate is raised in a careful manner so as to avoid any damage to the gel surface. The gel surface and the top plate are maintained parallel. The inertia of the geometry is calibrated by maintaining 1 mm thickness between the top plate and bottom surface, and then the top plate is raised. The polymer solution is then placed over the gel and the top plate is brought to the pre-set fluid thickness of 1 mm. We then allowed 10 min for the fluid temperature to be stabilized with the gel and its surroundings. The drying of the fluid at the circumference is prevented by covering the set up with an enclosure at the top.

To visualize the secondary flow pattern associated with the elastic instability, we used a custom-designed flow visualization arrangement shown in Figure 1. The base consists of a transparent glass plate supported by four equal size glass plates permanently fixed at the four sides. A mirror is kept under the transparent base plate at a 45 $^\circ$ angle with the bottom plate of the rheometer. The bottom surface of the upper shearing plate is coated with black ink to improve the contrast. Fluid is prepared by adding 0.5% of Kalliroscope particles (Kalliroscope Corp., Groton, MA) in the polymer solution and dispersed uniformly. The fluid is placed on the transparent plate and is uniformly illuminated from the bottom using a light source. This arrangement is used for visualizing and recording the secondary flow patterns associated with elastic instability for both fluid flow between rigid plates and flow on the gel surface. The polydimethyl siloxane (PDMS) gel used in our experiments is transparent. This gel allows light to pass through and illuminate the fluid flow, which helps in visualizing the actual fluid flow pattern on the gel surface. We have ensured that the tracer particles present in the fluid do not stick to the gel surface. A CCD camera (LU165C) is used to visualize and capture the sequence of patterns of secondary flow. The images are cropped and converted to gray scale, and are used for classifing the elastic instability modes, as done in the earlier work of Schiamberg *et al.*[10]

A. Fluid preparation and characterization

The polymer solution used in our experiments is polyacrylamide (of two different molecular weights, viz., $\sim 5 \times 10^6$ and 18×10^6 g mol^{-1}) dissolved in saccharose solutions at different concentrations, as summarized in Table I. Following Ref. 10, a required amount of polymer is uniformly dissolved (for 3 h) in deionized water using magnetic stirrer. Then saccharose and NaCl are added and thoroughly mixed (for 12 h) to get a homogeneous solution of 80, 200, 350, and 492 ppm polyacrylamide solutions with $M_w = 18 \times 10^6$ g mol^{-1}. We also used a second procedure (following Groisman and Steinberg[9]), where we prepare 100 and 300 ppm polyacrylamide ($M_w \sim 5 \times 10^6$ g mol^{-1}) solutions as follows. First, we prepared the polyacrylamide stock solution: 0.9 g of polyacrylamide is dissolved in 290 ml of deionized water and gently stirred for 3 h. Three

TABLE I. Rheological properties of various polymer solutions used in our experiments. Data observed at 25 °C, unless specified otherwise. The error-bars on the zero-shear (η_0) and solvent (η_s) viscosities are within 5% of the reported values. The polymer contribution to the solution viscosity is η_p. The relaxation time is determined by fitting the oscillatory-shear data with the single-mode Maxwell model.

Polymer concentration ppm	M_w of polymer g/mol	Saccharose concentration %	η_0 [Pa s]	η_s [Pa s]	λ [s]	$\beta = \eta_p/\eta_0$ ...
300	$\sim 5 \times 10^6$	58.5	0.23	0.06	2.9	0.74
100	$\sim 5 \times 10^6$	62.8	0.21	0.13	5	0.43
400	$\sim 5 \times 10^6$	65.9	0.74	0.19	12	0.74
300	$\sim 5 \times 10^6$	63	0.32	0.13	4.3	0.6
80 (at 12 °C)	18×10^6	65	0.4	0.28	3.6	0.30
200	18×10^6	65.9	0.32	0.19	6	0.41
350	18×10^6	65.9	0.6	0.19	7.4	0.68
492	18×10^6	65.9	1.5	0.19	18	0.86

grams of NaCl and 0.9 g of iso-propanol are uniformly dissolved in the solution. The solution is made up to 300 g by adding water, which has the final concentration of 3000 ppm polyacrylamide and this stock solution is diluted with the solvent to obtain solutions of different concentrations. Iso-propanol and NaCl are added to improve the solubility of polyacrylamide and prevent it from aging (following Ref. 9). The viscous Newtonian solvent is prepared by adding 65 g of saccharose, 1 g of NaCl, and 34 g of deionized water. The polymer solution for the flow experiments (300 ppm) is prepared by mixing 10 g stock solution and 90 g of solvent. For preparing the 100 ppm solution, 3.33 g of stock is mixed with 96.66 g of solvent. The sugar content of these solutions is 58.5% and 62.8% for 300 ppm and 100 ppm, respectively.

The solvents are characterized using the cone-and-plate geometry (diameter 60 mm, cone angle 0.035 radians) of the rheometer at 25 °C and the viscosities obtained (Figure 2(a)) for 65.9%, 62.8% and 58.5% saccharose are found to be 0.19, 0.13, and 0.06 Pa s, respectively, with an error bar of 5%. We have further verified that when the experiments are carried out at lower temperatures of 19 °C (Ref. 10) and 12 °C (Ref. 8), the obtained viscosity values are the same as those reported by earlier studies. The solvent clearly shows Newtonian behavior for three decades of shear rate and does not exhibit shear rate dependence of viscosity. In Figure 2(b), we show the stress as a function of time

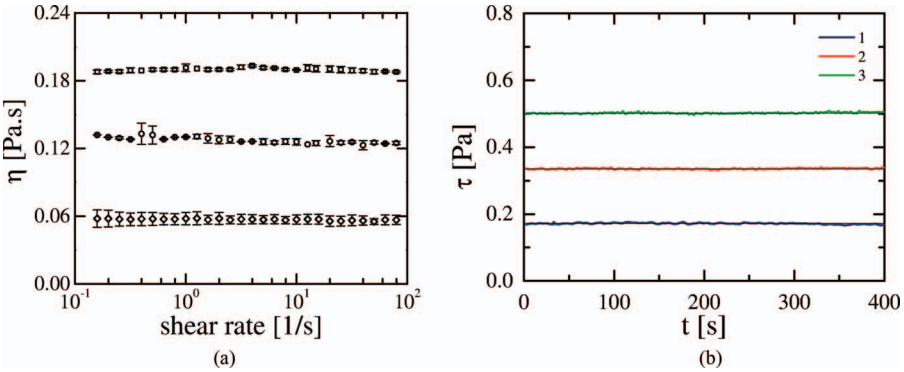

FIG. 2. Panel (a) shows the viscosities of the three solvents used in this study: 65.9% [open square], 62.8% [open circles], and 58.5% [open diamonds] saccharose dissolved with 1% NaCl in water. The measurements are performed using the cone-and-plate (60 mm diameter and cone angle of 0.035 radians) geometry at 25 ° C. Data clearly shows that the solvent viscosity is independent of shear rate. Panel (b) shows the stress vs time for the flow of solvent (obtained using the parallel-plate geometry), which contains 65.9% saccharose and 1% NaCl in water at 25 °C. The data correspond to shear rates of 1 (blue), 2 (red), and 3 (green) s^{-1}. For all the three shear rates, we have also plotted the time-averaged stress value using a thin black line. The stress in the pure solvent exhibits very little fluctuations with time. The values of the stress for different shear rates are: 0.172 ± 0.003 Pa ($\dot{\gamma} = 1\ s^{-1}$), 0.335 ± 0.007 Pa ($\dot{\gamma} = 2\ s^{-1}$), and 0.502 ± 0.002 Pa ($\dot{\gamma} = 3\ s^{-1}$).

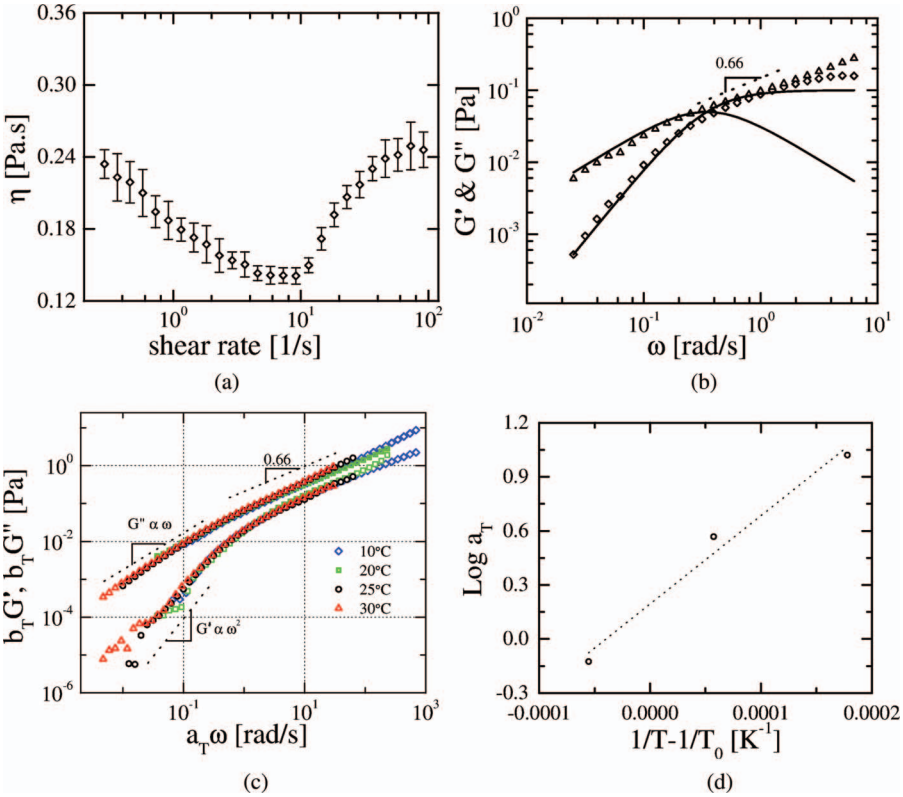

FIG. 3. Characterization of the 300 ppm polyacrylamide solution ($M_w \sim 5 \times 10^6$ g mol^{-1}) with 58.5% saccharose and 1% NaCl in water. The measurements are performed in a cone-and-plate geometry (60 mm diameter and cone angle 0.035 radians). Panel (a) contains the steady-shear data (at 25 °C) for viscosity as a function of shear rate. Panel (b) contains the oscillatory shear data (at 25 °C) showing $G'(\omega)$ (open diamonds) and $G''(\omega)$ (open triangles). The curves show the best fit of the data to a single-mode Maxwell model. Panel (c) contains the master curve of $G'(\omega)$ and $G''(\omega)$ as a function of $a_T\omega$ obtained from data at $T = 10$, 20, 25, and 30 °C. Panel (d) shows the Arrhenius plot for temperature dependence of a_T. See text for explanation of symbols and additional details. (a) Steady-shear data, (b) oscillatory shear data, (c) time-temperature superposition, and (d) temperature dependence of frequency shift parameter a_T.

for the pure solvent, and this shows that at different shear rates, the stress is independent of time, thus indicating the viscometric (laminar) nature of the solvent flow. This behavior is subsequently used to contrast (later in Sec. III B) the time-dependent behavior of stress the torsional flow of the polymer solution.

The polymer solutions are also characterized (Figure 3) by using the cone-and-plate geometry of the rheometer at 25 °C. We used steady-shear experiments to characterize the zero-shear viscosity, and small-amplitude oscillatory shear experiments to characterize the longest relaxation time λ of the polymer solution (in the linear stress regime of 0.05 Pa). The zero-shear viscosity, η_0, the longest relaxation time (λ) of the polymer solution, and solvent viscosities are summarized in Table I. Figure 3(a) shows the steady-shear viscosity as a function of shear rate for the 300 ppm polyacrylamide solution ($M_w \sim 5 \times 10^6$ g mol^{-1}), and this indicates that there is shear thinning of the viscosity of the solution initially, but at higher shear rates, there is an apparent shear thickening due to the onset of the purely elastic instability. Figure 3(b) shows the shear modulus $G'(\omega)$ and the loss modulus $G''(\omega)$ as a function of frequency. We fit the results from oscillatory shear data, viz., $G'(\omega)$ and $G''(\omega)$ with the single-mode Maxwell model as follows. The polymer contribution to G' and G'' is given by the single-mode Maxwell model as

$$G'(\omega) = \frac{g_1\lambda^2\omega^2}{1+\lambda^2\omega^2}, \qquad G''(\omega) = \frac{g_1\lambda\omega}{1+\lambda^2\omega^2},$$

where g_1 and λ are parameters of the single-mode Maxwell model that must be obtained by fitting with experimental data. The parameter λ is the longest relaxation time of the polymer solution. As shown by Figure 3(b), at frequencies smaller than the crossover frequency, we find that the data obey the terminal behavior $G'(\omega) \propto \omega^2$ and $G''(\omega) \propto \omega$ characteristic of polymer solutions. At higher frequencies, we find that G' and $G'' \propto \omega^{2/3}$ agree with the Zimm model predictions for dilute polymer solutions. The single-mode Maxwell model parameters g_1 and λ are fitted to the data, and for Figure 3(b), we find that $g_1 = 0.1$ Pa and $\lambda = 2.9$ s. The same procedure is followed to characterize the relaxation times of the various polymer solutions used in this study. The data are summarized in Table I. We also carried out measurements of $G'(\omega)$ and $G''(\omega)$ in the frequency range 6×10^{-3}–60 rad/s at four different temperatures 10, 20, 25, and 30 °C, and carried out the time-temperature superposition[23] of this data by plotting $b_T G'(\omega)$ and $b_T G''(\omega)$ with $a_T\omega$ (Figure 3(c)). Here a_T is the horizontal (frequency) shift factor which is theoretically given by $\eta_T T_0/(\eta_{T_0} T)$, where η_T is the zero-shear viscosity of the polymer solution at temperature T, while η_{T_0} is the zero-shear viscosity at the reference temperature T_0 (taken to be 25 °C). The theoretical value of the vertical shift factor $b_T = T_0\rho_0/(T\rho)$. In our data, the a_T and b_T values obtained from the theoretical expression did not give rise to a perfect superposition, and values were adjusted to obtain the master curve. The actual values of a_T used are plotted as a function of inverse temperature in an Arrhenius plot in Figure 3(d). From the slope of this plot, the activation energy is estimated to be around 40 kJ/mol.

To benchmark our procedure in characterizing the rheology of the polymer solutions, we also prepared polymer solutions identical (in polymer concentration, molecular weight, and solvent condition) to those used in the earlier work of Groisman and Steinberg.[8] The solvent (65% saccharose and 1% NaCl in water) viscosity is obtained at 12 °C is 0.324 Pa s, which agrees well with Groisman and Steinberg.[8] We added 80 ppm polyacrylamide ($M_w = 18 \times 10^6$ g mol^{-1}) to the solvent and the observed viscosity of the solution is 0.402 Pa s at 1 s^{-1} in the steady state mode, which is close to the reported value of 0.424 Pa s. We estimated the relaxation time of this solution (using the method described above) to be 3.6 s, which is close to reported value of 3.5 s in Ref. 8.

B. Preparation and characterization of the soft solid layer

The composition of the PDMS gel used consists of the elastomer base 8%, cross-linker (curing agent) 2% (Sylgard 184 elastomer, Dow Corning©), and silicone oil 90% (Dow Corning© 200 Fluid). These constituents are added in a beaker and thoroughly mixed with a spatula to obtain a homogeneous mixture. Degassing is done in a desiccator connected to a vacuum pump to remove entrapped air, if any. Care is taken to avoid overflow of the solution due to the expansion of air bubbles during degassing. The degassed solution appears completely clear and transparent without air bubbles. A template is prepared by taking plain glass plate of side 7.5 cm × 7.5 cm, on which microscope glass slides (1 mm thickness) of 1 cm width and 7.5 cm length are pasted in the edges by thin double sided tape so as to have a rectangular well (5.5 cm × 5.5 cm) ranging from 2 to 10 mm thickness. The degassed mixture is dispensed carefully on the template to avoid air entrapment in the process. The template is kept horizontal during the dispense, and then placed in a pre-heated oven, where curing is done at 70 °C for 12 h. Other PDMS gels with 5% and 10% cross-linker concentration (without silicone oil) are also prepared similarly.

The linear viscoelastic properties of the gel are determined using the parallel plate geometry of the rheometer. The gel slab is placed on the bottom plate and the top plate is brought in contact with the gel surface till the bottom plate sensed a normal force of 0.45 N, which is taken as an indicator of zero gap between the top plate and the gel surface. The rheometer is operated in the oscillatory mode, wherein oscillatory stress is applied to the top plate and angular displacement is measured. The frequency spectrum of the shear modulus is shown in the Figure 4 in the range 0.0628–62.8 rad/s. The rheological properties of the PDMS gel slabs used in our experiments are summarized in Table II. The results for G' and G'' from our experiments agree well with those reported in Ref. 20 prepared under identical conditions. The bulk (compression) modulus K is measured using the AR1000-N rheometer using the protocol similar to the one described in Ref. 20. Here, the parallel-plate configuration is used, and the top plate is lowered with a specified vertical displacement, and the corresponding normal force is recorded by the rheometer. The ratio of normal

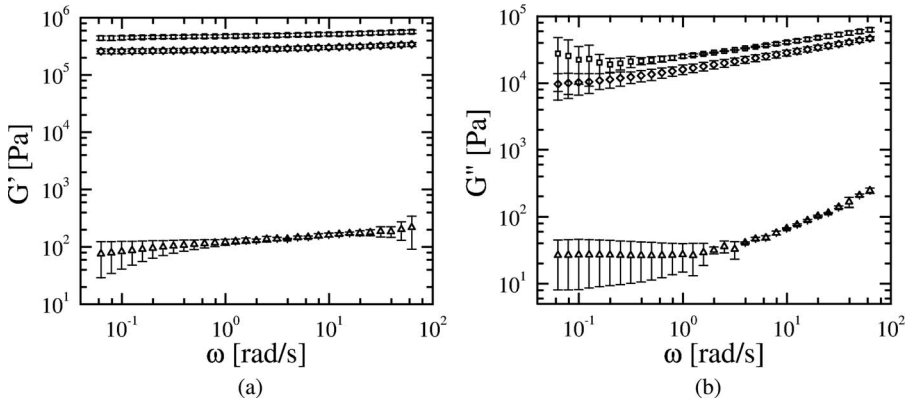

FIG. 4. Characterization of the three different PDMS gels: Storage modulus $G'(\omega)$ (panel (a)) and loss modulus $G''(\omega)$ (panel (b)) for the 2% [open triangle], 5% [open diamond], and 10% [open square] cross-linker PDMS gels. The measurements are performed using the parallel-plate geometry at 25 °C. The thickness of the gels used are 2 mm and 4 mm.

stress to normal strain is the bulk (compression) modulus of the gel. The data for K as a function of cross-linker concentration are shown in Figure 5. For the 5% and 10% cross-linker gels, the values of K are in good agreement with those reported in Ref. 20. It must be mentioned that we are only able to measure the zero-frequency value of K in the linear stress regime. It is possible that the value of K will vary with compressive strain at higher values of the strain.

III. EXPERIMENTAL RESULTS

In this section, we describe the experimental observations for the flow of polyacrylamide solution over both rigid surfaces and PDMS gels. Before carrying out experiments in flow past PDMS gels, we first carried out extensive experiments in the torsional flow of polymer solutions in various rheometer configurations without the gel. In the parallel-plate and cone-and-plate geometries, we find purely elastic instabilities at much lower shear rates compared to earlier experiments,[10] but the temperature in our experiments is close to 25 °C, unlike earlier works. A representative plot of the manifestation of this instability is shown in Figure 6. In this figure, we show data for the apparent viscosity as a function of $Wi = \dot{\gamma}\lambda$ for both parallel-plate and concentric cylinder geometries at 25 °C in the shear rate-controlled mode. At a fixed value of shear rate, the stress is measured at intervals of 1 s, and the stress value corresponding to the fixed shear rate is recorded only when four consecutive stress values is within 5% of the running average of the stress. We repeated the experiments on four different samples (with identical composition) for a given shear rate, and the average viscosity value is plotted in Figure 6. When the flow is viscometric, the zero-shear viscosity values agree for both parallel-plate and the concentric cylinder geometries. However, for the parallel-plate geometry, the apparent viscosity shows a sharp increase near $Wi \sim 3$, indicating the onset of the purely elastic instability. After the onset of instability, at a given shear rate, the stress in the solution shows large fluctuations (discussed later in Figure 11(a); also seen in Refs. 6 and 10) as

TABLE II. Rheological properties of PDMS gels (at 25 °C) used in this study. The shear and loss modulus data are averaged over the frequency range 0.062 to 62 rad/s. The data for bulk modulus K are also presented.

	2% cross-linker gel	5% cross-linker gel	10% cross-linker gel
G' [kPa]	0.13 ± 0.03	289 ± 25	494 ± 36
G'' [kPa]	0.06 ± 0.05	2 ± 1	3 ± 1
K [kPa]	1.8 ± 0.6	3200 ± 1000	3500 ± 1000

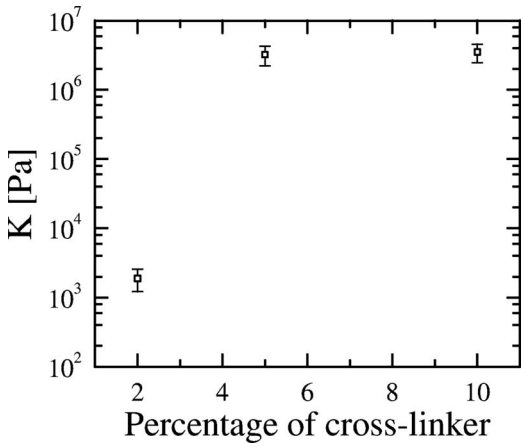

FIG. 5. The bulk (compression) modulus for various gels (at 25 °C) as a function of the % cross-linker. The parallel-plate geometry of the rheometer is used, and the thicknesses of the gels used are 2 mm and 4 mm.

a function of time. Hence, a steady (apparent) viscosity value cannot be recorded at a fixed shear rate. In Figure 6 (and subsequent figures), we show the average value of the stress (average taken over 10 min of data) at a given shear rate. The spread of data (in the unstable regime) about the average as represented by the standard deviation is at most 25%. It must be noted that this spread is a genuine physical phenomenon, and is not due to experimental measurement error. However, the apparent viscosity (in Figure 6) obtained from the concentric cylinder geometry continues to shear thin, and shows an abrupt increase only at much higher shear rates. In the Appendix, we provide a detailed characterization of this instability, and demonstrate that this is indeed a purely elastic instability. In Sec. III A, we discuss the experimental observations for the flow of polyacrylamide solutions past both soft (2% cross-linker) and relatively hard (5 and 10% cross-linker) PDMS gels, and show that the elastic instability is suppressed at intermediate shear rates only for the soft (2% cross-linker) PDMS gels. Section III B deals with the time-dependent variation of stress at fixed shear rates, and Sec. III C deals with discussion of results from visualization of the flow using tracer particles.

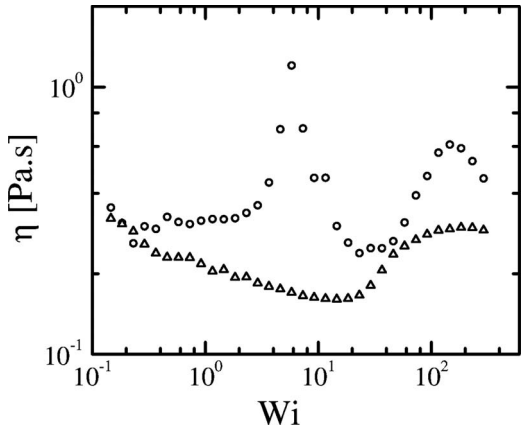

FIG. 6. Illustration of purely elastic instability in polymer solution flow (controlled shear-rate mode) past a rigid surface at 25 ° C. Plot shows the apparent viscosity vs Weissenberg number (Wi) for the 300 ppm polyacrylamide ($M_w \sim 5 \times 10^6$ g mol^{-1}) solution with 58.5% saccharose and 1% NaCl in water. The open circles denote data for the parallel-plate geometry (aspect ratio $d/R = 0.05$) and open triangles denote data for the concentric cylinder geometry (inner diameter 28 mm and fluid thickness of 1 mm). The relaxation time λ of the solution is 2.9 s. The purely elastic instability at lower shear rates is absent in the concentric cylinder geometry. The error bars for the apparent viscosity in the viscometric regime is at most 5%, while the spread of the data in the unstable regime has standard deviation of at most 25%.

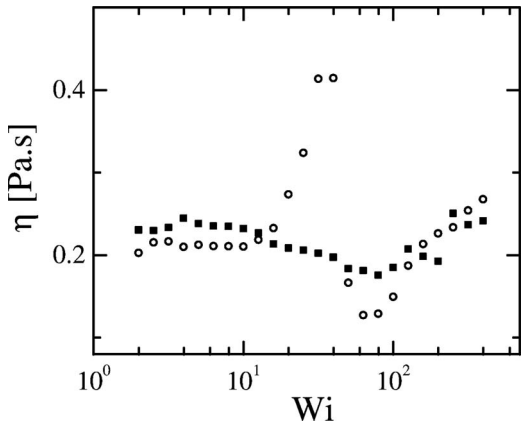

FIG. 7. Data showing suppression of purely elastic instability over a gel: Apparent viscosity versus Wi for the flow of 100 ppm polyacrylamide solution ($\lambda = 5$ s, $M_w \sim 5 \times 10^6$ g mol^{-1}) between parallel plates (open circles) and over the PDMS gel (closed squares). The fluid aspect ratio $d/R = 0.05$, and the gel to fluid thickness $H/d = 10$. The gel has 2% concentration cross-linker mixed with silicone oil and the plateau modulus $G' = 0.13 \pm 0.03$ kPa. The non-dimensional elasticity of the gel is given by $\eta_0/(G'\lambda) = 3.1 \times 10^{-4}$. The error bars for the apparent viscosity in the viscometric regime is at most 5%, while the spread of the data in the unstable regime has standard deviation of at most 25%.

A. Flow of polymer solutions over soft and relatively harder gels

Having established (in the Appendix) that the initial viscosity increase is indeed due to the purely elastic instability in flow between parallel plates, we next proceed to understand the role of gel deformability on the purely elastic instability. We first used the 100 ppm polyacrylamide solution ($M_w \sim 5 \times 10^6$ g mol^{-1}, $\lambda = 5$ s) dissolved in 62.8% saccharose and 1% NaCl in water. In Figure 7, we show the apparent viscosity for the steady flow between parallel plates which exhibits elastic instability, and for flow over the soft PDMS gel (2% cross-linker). The thickness of the PDMS gel is 10 mm and its shear modulus is 0.13 ± 0.03 kPa. The rheometer is operated in rate-controlled mode in the range 0.1 to 100 s^{-1} corresponding to a Weissenberg number range of 0.5–500, and a Reynolds number range of 0.0005 to 0.5. The low-shear viscosity as function of shear rate is constant for a decade for the flow between rigid surfaces and on the gel, and there is good agreement for the apparent viscosity with and without the gel. There is a slight deviation in the low-shear viscosity value, and this was also observed in the earlier experiments on Newtonian fluid flow past a soft gel.[16] We observed a gradual increase in apparent viscosity (shear thickening) at 2 s^{-1} for the flow between rigid surfaces. However, for flow of the polymer solution over the gel, no shear thickening is observed at 2 s^{-1}, and the fluid continues to shear thin until a shear rate of about 10 s^{-1}, after which the apparent viscosity for both experiments are similar. For the parameters studied in Figure 7, we estimated the non-dimensional parameter $\Gamma/Wi = \eta_0/(G'\lambda) \sim 3.1 \times 10^{-4}$ using the zero-shear viscosity of the polymer solution. The parameter Γ represents the ratio of viscous stresses in the flow to the elastic stresses in the solid, and signifies the measure of deformability in the solid. Previous studies[17,19,21] have used this parameter to analyze the effect of solid deformability on the instability of a Newtonian fluid past a soft solid surface, and they have demonstrated the interface is unstable if Γ is greater than a $O(1)$ number. But the parameter Γ depends on the shear rate, just as Wi does. Hence, we found it appropriate to introduce the shear rate independent ratio $\Gamma/Wi = \eta_0/(G'\lambda)$ to characterize the deformability of the solid. For the parameters reported in Figure 7, the theoretical prediction for the flow-induced interfacial instability (of a Newtonian fluid) is $\Gamma = 0.3$. In an earlier work,[21] it was shown that the effect of viscoelasticity of the polymer solution is to increase this value (i.e., viscoelasticity of the solution stabilizes the instability of the interface between the fluid and the gel) compared to the Newtonian fluid value. Thus, in our experiments, the operating conditions are such that Γ is well below the value required for the flow-induced interfacial instability. It is therefore not clear whether Γ value of 0.003 could be large enough for the solid to deformed by the shear stresses exerted by the fluid. In addition to the shear modulus, the bulk (compression)

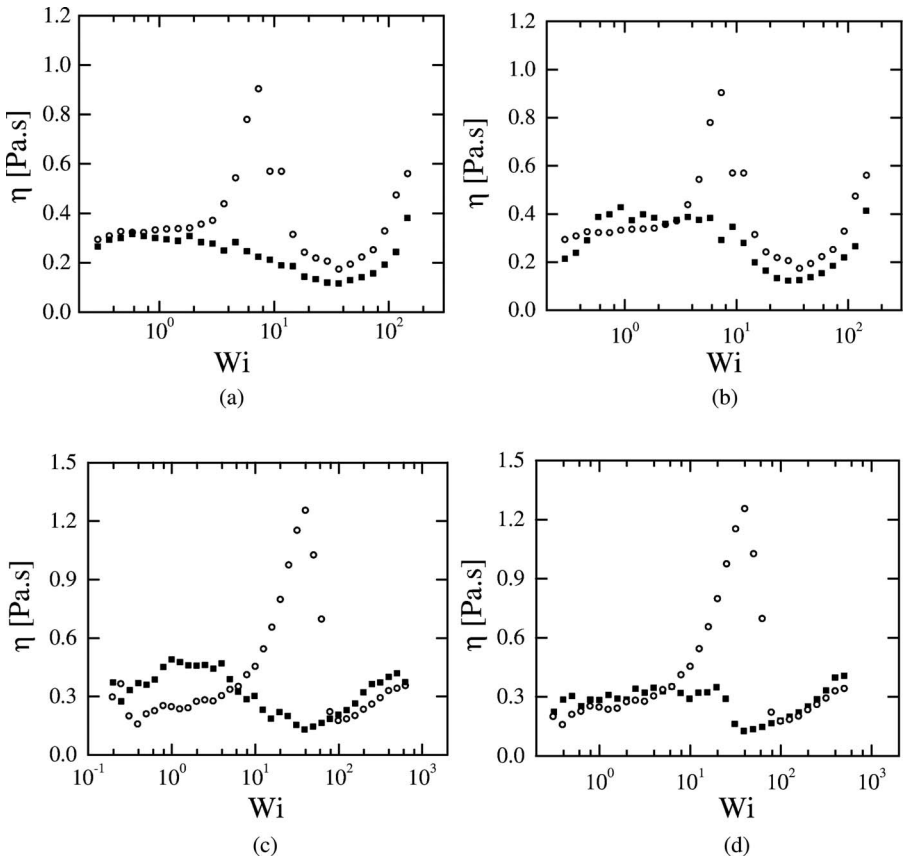

FIG. 8. Instability suppression in flow over a gel: Apparent viscosity versus Wi for the flow of 300 ppm polyacrylamide solution ($M_w \sim 5 \times 10^6$ g mol^{-1}, $\lambda = 2.9$ s) with 58.5% saccharose and 1% NaCl dissolved in water. Figure shows results for flow between rigid parallel plates [open circle] and over the 2% PDMS gel [closed square], respectively. The aspect ratio $d/R = 0.05$. Panels (a) and (b) show results obtained using the rate-controlled mode and panels (c) and (d) show results obtained using the stress-controlled mode. In panels (a) and (c), $H/d = 2$, and in panels (b) and (d) $H/d = 4$. The non-dimensional gel elasticity $\eta_0/(G'\lambda) = 5.8 \times 10^{-4}$. The error bars for the apparent viscosity in the viscometric regime is at most 5%, while the spread of the data in the unstable regime has standard deviation of at most 25%.

modulus of the gels is also measured (Table II), and for the softest gel prepared (2% cross-linker), $K \sim 1.8$ kPa, and it is possible that the first-normal stress difference exerted by the polymer solution compresses the gel significantly. We explore this hypothesis further in Sec. IV, and argue that this compression of the gel provides a consistent explanation of the suppression of the purely elastic instability in flow past gels.

We next carried out experiments with 300 ppm polyacrylamide solution prepared in 58.5% saccharose and 1% NaCl in water. The rheometer was operated in the rate-controlled mode in the range 0.1 to 100 s^{-1} (Wi range 0.29 to 290 and Reynolds number range 0.0004 to 0.4), as well as in the stress-controlled mode. In Figure 8, we show the steady state viscosity for both rate-controlled and stress-controlled experiments for flow over gels of different thickness and for flow over the rigid rheometer plate. The Wi for the stress-controlled experiment is calculated by estimating the shear rate as τ/η_0, and by using this value of the shear rate in the definition of Wi. For flow between rigid plates, we observe shear thickening of the apparent viscosity at $Wi = 2.9$. However, the flow of polymer solution over the soft gel does not exhibit shear thickening at $Wi = 2.9$. The apparent viscosity for flow over a gel continues to shear thin up to $Wi = 29$, and for $Wi > 29$, the apparent viscosity is identical to flow between rigid plates. The absence of shear thickening is also observed for gels of different thickness viz., 2 and 4 mm. To confirm that this feature is present in the stress-controlled mode, we applied stresses in the range of 0.1 to 50 Pa. The apparent shear thickening was observed at $Wi \sim 5$ for flow between rigid surfaces, which was absent for flow over a gel. The

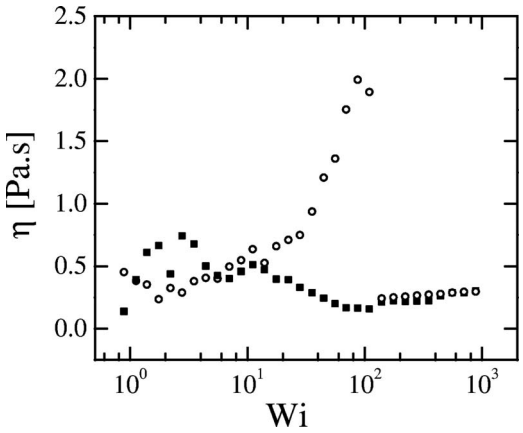

FIG. 9. Instability suppression in flow past a gel in the parallel-plate geometry: Apparent viscosity as function of Wi for the 80 ppm ($M_w = 18 \times 10^6$ g mol^{-1}; $\lambda = 3.6$ s) polymer solution flow over rigid surface (open circle) and 2% cross-linker PDMS ($H/d = 2$) gel surface (closed square). Aspect ratio $d/R = 0.075$, and the non-dimensional gel elasticity $\eta_0/(G'\lambda) = 1 \times 10^{-3}$. The error bars for the apparent viscosity in the viscometric regime is at most 5%, while the spread of the data in the unstable regime has standard deviation of at most 25%.

critical Weissenberg numbers for onset of instability in rigid surfaces are in reasonable agreement for the rate- and stress-controlled experiments. The viscosity behavior for flow over a gel is identical to that in rigid surfaces at higher Wi. Thus, the suppression of the purely elastic instability by the gel is independent of the specific mode of operation of the rheometer, and it depends only on fluid and soft solid properties, thickness of the fluid and soft solid.

To examine the effect of molecular weight of the polymer solution on the elastic instability and its suppression, experiments on flow over a gel have been carried out with 80 ppm ($M_w = 18 \times 10^6$ g mol^{-1}, $\lambda = 3.6$ s) polyacrylamide (Polysciences, Warrington, PA) in 65% sugar solvent. The measurement is obtained using parallel plate geometry with a low aspect ratio $d/R = 0.075$, which is the maximum fluid thickness possible in this geometry of the rheometer. Figure 9 shows the steady flow of polymer solution, where increase in viscosity begins at $Wi \sim 3.6$. We observe the absence of elastic instability flow over the 2 mm gel (2% cross-linker) at $Wi \sim 3.6$. This experiment is carried out with stress-controlled mode for a solution composition similar to one used by Groisman and Steinberg.[8] To further support our hypothesis that the suppression of the purely elastic instability is due to the altered flow induced by the deformability of the gel, we carried out control experiments wherein we used relatively hard (shear modulus $G' = 289 \pm 25$ kPa, compression modulus $K = 3200 \pm 1000$ kPa and $G' = 494 \pm 36$ kPa, $K = 3500 \pm 1000$ kPa) PDMS gels (thickness 2 and 4 mm). In Figure 10, we show shear rate versus apparent viscosity for flow over the two different harder PDMS gels as well as without the PDMS gel. There is a slight variation in the zero-shear viscosity values for flow between the rheometer plates and over a gel. At higher shear rates, the flow of polymer solution over the relatively hard PDMS gels shows the elastic instability trend similar to flow between rigid parallel plates. We find a similar increase in viscosity at a shear rate near $Wi \sim 3$, in agreement with flow over rigid surfaces. The disappearance of the viscosity bump in the flow over the very soft PDMS (2% cross-linker) gel ($G' = 0.13 \pm 0.03$ kPa, $K = 1.8 \pm 0.6$ kPa) observed earlier can thus be unambiguously attributed to the flow modification due to the deformation of the gel.

B. Time-dependent stress change for polyacrylamide solution flow on soft and hard PDMS gels

We next discuss the temporal variation of the stress at a given shear rate for (1) flow between two parallel plates of the rheometer, (2) for flow over the soft gel with $G' \sim 0.13$ kPa (2% cross-linker), and (3) for flow over the harder PDMS gels with $G' \sim 289$ (5% cross-linker) and 494 (10% cross-linker) kPa. To probe the nature of the altered flow on the gel, the instantaneous stress

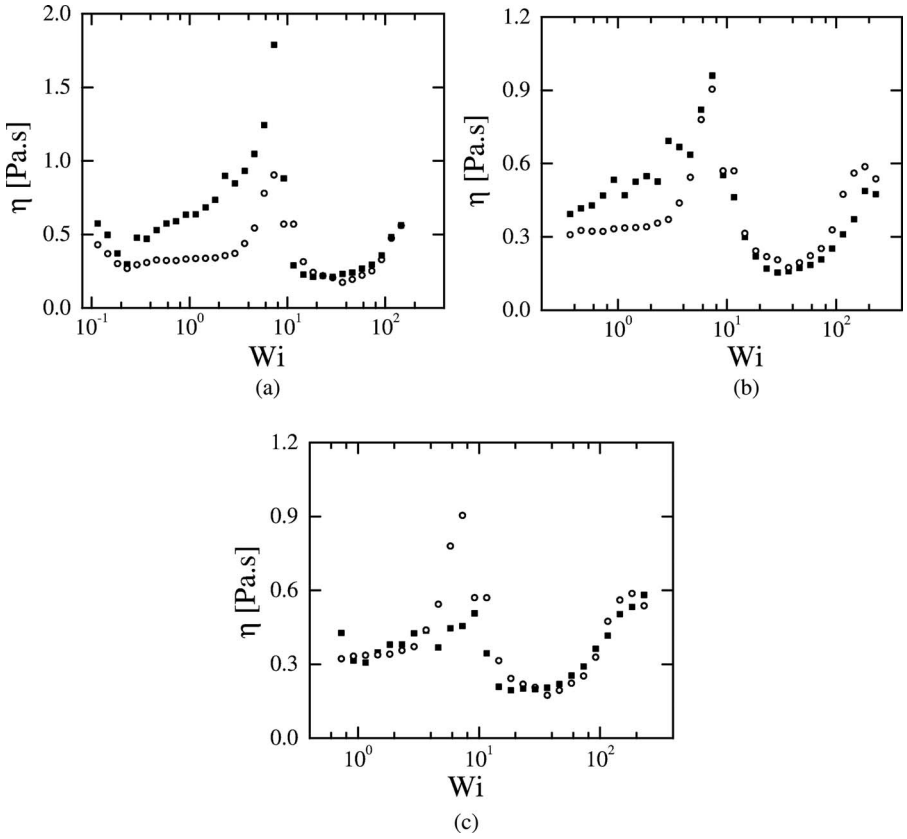

FIG. 10. Absence of instability suppression in the flow over relatively harder PDMS gels: The fluid is 300 ppm polyacrylamide solution dissolved with 58.5% saccharose and 1% NaCl in water ($\lambda = 2.9$ s; $M_w \sim 5 \times 10^6$ g mol^{-1}). Panel (a) shows the flow of polyacrylamide solution over 4 mm thickness PDMS (5% cross-linker; $H/d = 4$) gel with shear modulus 0.29 $\pm$ 0.03 MPa and bulk modulus 3.2 $\pm$ 1 MPa. Panels (b) and (c) show the flow of polyacrylamide solution on 2 and 4 mm thickness PDMS (10% cross-linker) gel with shear modulus 0.49 $\pm$ 0.04 MPa and bulk modulus 3.5 $\pm$ 1 MPa, respectively. Closed square indicates the flow on the harder PDMS gels, and open circle indicates flow between rigid parallel plates. Aspect ratio $d/R = 0.05$; Fluid thickness = 1 mm. The values of $\eta_0/G'\lambda = 2.75 \times 10^{-7}$ for panel (a), and $\eta_0/G'\lambda = 1.61 \times 10^{-7}$ for panels (b) and (c). The error bars for the apparent viscosity in the viscometric regime is at most 5%, while the spread of the data in the unstable regime has standard deviation of at most 25%.

measured by the rheometer as a function of time is observed at constant shear rate steps, ranging from 0.25 to 50 s^{-1}. For each shear rate, the stress change is observed for 600 s at 1 s intervals. In Figure 11(a), we show time-dependent stress variation for the flow of 300 ppm polymer solution between the rigid plates of the rheometer. The bottom black line shows nearly constant stress for controlled $Wi = 0.29$, which indicates the flow is viscometric for this shear rate. Flow of the polymer solution between rigid plates shows highly irregular stress variation with time due to the instability and due to the resultant secondary flow for $Wi = 2.9$ and 5.8. The average value of the stress in the solution is 1.15 and 1.74 Pa, respectively, for $Wi = 2.9$ and 5.8. The time-dependent stress variation for flow on the gel (2% cross-linker; $H/d = 2$) at different Wi is shown in Figure 11(b). For $Wi \sim 2.9$, the stress fluctuates about an average value of 0.6 Pa, while at $Wi = 5.8$, the stress fluctuates around 0.85 Pa. When compared to the rigid surface, the magnitude of the stress fluctuations have decreased in flow over a gel, and this feature is repeatable. This trend is true only in the shear rate range where the apparent viscosity is different for flow between rigid plates and flow over a gel. This trend is also observed (Figure 11(c)) for a different gel thickness of $H/d = 4$. The average time-dependent shear stress values for the 300 ppm polyacrylamide solution for both rigid surfaces and flow over a gel are summarized in Table III. The average stress values for a rigid surface are higher compared to the average stress values for flow over the soft gel at a given shear rate, suggesting that the instability is indeed suppressed in the flow over a gel. In contrast,

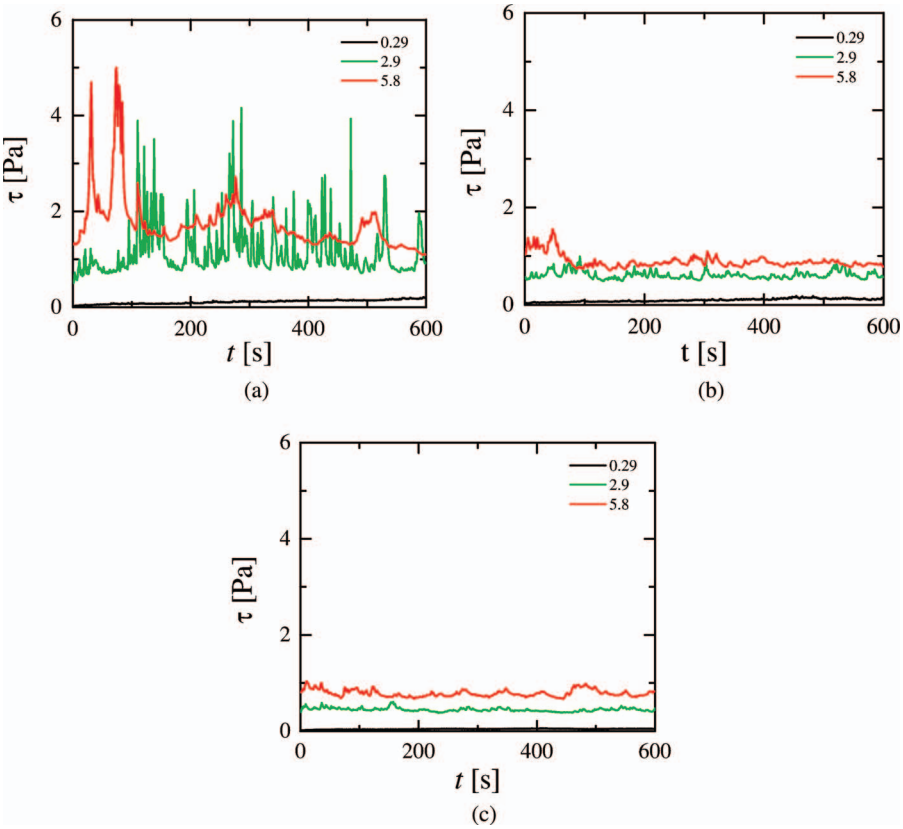

FIG. 11. Absence of stress fluctuations in flow over the gel: Time-dependent stress variation for the flow of 300 ppm polyacrylamide solution (prepared with 58% saccharose; $M_w \sim 5 \times 10^6$ g mol^{-1}) between parallel plates (panel (a)) and flow over the 2% cross-linker PDMS gel (panels (b) and (c)) at constant Wi of 2.9 (green) and 5.8 (red). Panels (b) and (c) show the flow over gels with thickness $H/d = 2$ and 4, respectively. The black line at the bottom indicates the stress variation under laminar conditions for $Wi = 0.29$, $\Gamma/Wi = \eta_0/(G'\lambda) = 5.8 \times 10^{-4}$.

the average stress values for flow over the relatively hard PDMS gels (5% and 10% cross-linker) is comparable to the rigid surface value indicating that the suppression of the instability is driven by the gel deformability in the case of the soft gel (2% cross-linker).

As discussed in Sec. III A, at shear rates greater than 10 s^{-1}, the apparent viscosity for flow over the soft gel and rigid plate coincides. This suggests that the deformability of the gel is not sufficient enough to modify the flow, and the elastic effects in the bulk of the fluid dominate the flow and the accompanying instabilities. This inference is borne out by the stress vs time data for different shear rates (in the range 4–10 s^{-1}) shown in Figure 12. This shows that at shear rates > 4 s^{-1}, the stress fluctuations are quite similar in flow between rigid plates and flow over the 2% cross-linker gel. In Figure 13, we show the stress vs time data for flow between rigid plates, flow over the soft gel (2% cross-linker) as well as for the harder gel (5% cross-linker) at the same $Wi = 2.9$. This clearly shows that the stress fluctuations are completely absent for the soft PDMS (2% cross-linker) gel, while the fluctuations are markedly predominant for both the harder PDMS gel (5% cross-linker) and the flow

TABLE III. Average time-dependent shear stress values [Pa] for controlled shear rate.

Wi	Rigid	2 mm gel 2% cross-linker	4 mm gel 2% cross-linker	10 mm gel 2% cross-linker	2 mm gel 5% cross-linker	4 mm gel 5% cross-linker	10 mm gel 5% cross-linker
2.9	1.152	0.61	0.45	0.54	2.73	2.78	0.66
5.8	1.742	0.85	0.79	0.92	2.25	2.47	1.16

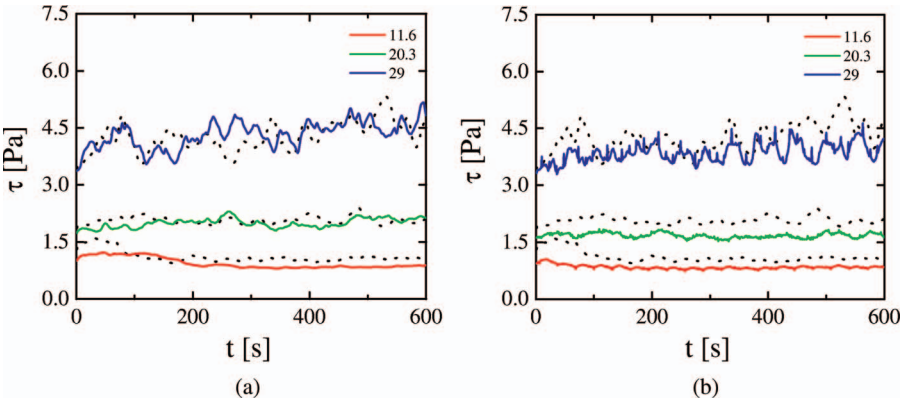

FIG. 12. Illustration of appearance of stress fluctuations in flow over the 2% cross-linker gel at higher shear rates. Figure shows time-dependent stress variation for the flow of 300 ppm polymer solution ($M_w \sim 5 \times 10^6$ g mol^{-1}, $\lambda = 2.9$ s, prepared with 58.5% saccharose and 1% NaCl in water) at different values of $Wi = 11.6$ (red), 20.3 (green), and 29 (blue) over the gel. The results for flow over a rigid surface are also shown (black dotted lines corresponding to each Wi). Panels (a) and (b) show results for polymer solution flow over gels with $H/d = 2$ and 4, respectively. Aspect ratio $d/R = 0.05$, $\Gamma/Wi = \eta_0/(G'\lambda) = 5.8 \times 10^{-4}$.

over the rigid bottom plate. These fluctuations are associated with concentric ring pattern for shear rate 1 s^{-1}, which described below in the flow visualization section.

Hysteresis experiments (following McKinley *et al.*[4]) are carried out in the rate-controlled mode, wherein we observe the variation of apparent viscosity with time at a given shear rate for the 300 ppm polymer solution. The shear rate is initially maintained for 1200 s at $Wi = 1.45$, which is lower than the critical Wi for instability. Then Wi is increased to 5.8, and the flow is kept at this shear rate for 1200 s, and the system is again brought back to the $Wi = 1.45$. If the system did not exhibit hysteresis, the apparent viscosity of the system at $Wi = 1.45$ would be same before and after the high-shear rate regime. However, if the system exhibited hysteresis, the apparent viscosity would be different at the $Wi = 1.45$ before and after the high-shear rate regime. In Figure 14, we show the apparent viscosity variation as a function of time for flow between parallel plates, and for flow of polymer solution over the gel (2% cross-linker) surface. For flow between rigid plates, when Wi is increased from 1.45 to 5.8, the apparent viscosity increases (due to the instability), and when Wi is reduced again to 1.45, the apparent viscosity value takes a very different value. In marked contrast,

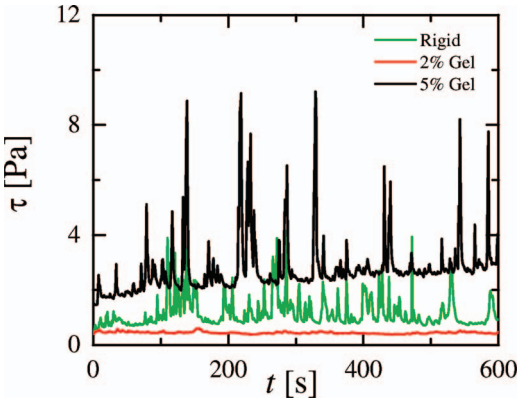

FIG. 13. Stress fluctuations in the flow of polymer solution over rigid surface and gels of different shear moduli: Time-dependent stress variation for the flow (at $Wi = 2.9$, aspect ratio $d/R = 0.05$) of 300 ppm polymer solution ($M_w \sim 5 \times 10^6$ g mol^{-1}, $\lambda = 2.9$ s) over the 2% cross-linker gel (red; $H/d = 4$; $\Gamma/Wi = \eta_0/(G'\lambda) = 5.8 \times 10^{-4}$), 5% cross-linker gel (black; $H/d = 4$, $\Gamma/Wi = \eta_0/(G'\lambda) = 2.75 \times 10^{-7}$), and the rigid bottom surface of the rheometer (green). While the stress fluctuations are predominant for flow over the rigid surface and the 5% cross-linker gel, they are minimal for flow over the 2% cross-linker gel, demonstrating the suppression of instability in the flow over 2% cross-linker gel.

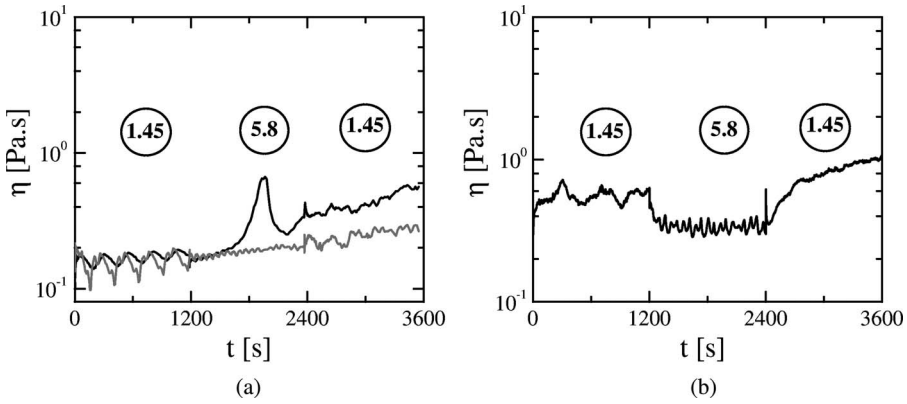

FIG. 14. Presence or absence of hysteresis for flow over a rigid plate, and for flow over the gel: Apparent viscosity as a function of time for (a) flow of 300 ppm polyacrylamide solution ($M_w \sim 5 \times 10^6$ g mol^{-1}, $\lambda = 2.9$ s) between parallel rigid plates at $Wi = 1.45$ and 5.8, (b) flow of polymer solution over 2% cross-linker PDMS gel with $H/d = 2$, $\Gamma/Wi = \eta_0/(G'\lambda) = 5.8 \times 10^{-4}$. The bottom (gray) line in figure (a) shows the viscosity of pure solvent, which shows less fluctuations.

for flow over a gel, when the Wi increased as above, the viscosity decreases, and upon subsequent decrease in Wi, the viscosity approximately regains its original value. Our results thus clearly show that flow past the soft gel surfaces does not exhibit hysteresis, while flow between rigid plates shows significant hysteresis.

C. Flow visualization

We next discuss the features observed during flow visualization in the presence and absence of various gel layers. Visualization of the flow of 300 ppm polyacrylamide solution between the transparent bottom plate and rotating top plate is carried out for aspect ratio of 0.075. We then visualized the flow over 4 mm soft PDMS gel (G'= 0.13 kPa) and the harder PDMS gel with G'=494 kPa. The soft and hard PDMS gels are both transparent which helps in visualizing the flow pattern in the solution. Instability pattern for flow of polymer solution for $Wi = 2.9$ is shown in the Figure 15. The concentric ring pattern (Figure 15(a)) spreads in space between the center and the edge of the fluid, which resembles the axisymmetric mode of elastic instability patterns reported in Ref. 6. This axisymmetric elastic instability pattern disappears (Figure 15(b)) for flow on 4 mm soft (2% cross-linker) gel while the instability pattern is present for the hard (10% cross-linker) PDMS gel Figure 15(c). Concentric ring patterns appear for flow on the rigid surface (and the 10% cross-linker gel) but not for flow on the 2% cross-linker gel, which serves as a clear visual evidence

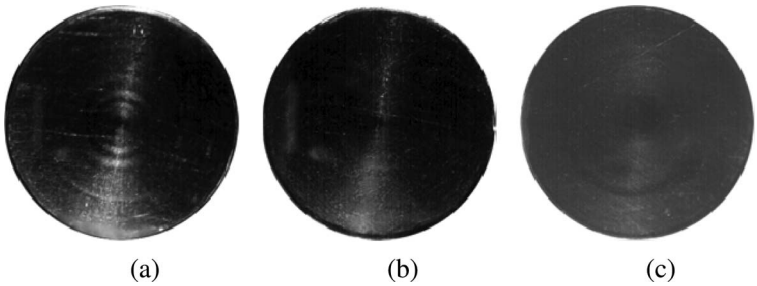

FIG. 15. Representative snapshots of the flow of 300 ppm polymer solution (at 25 °C, $M_w \sim 5 \times 10^{-6}$ g mol^{-1}, $\lambda = 2.9$ s) over rigid and gel surfaces (as viewed from the bottom side of the rheometer). The flow is visualized by seeding the fluid with light reflecting flakes. (a) Elastic instability pattern at $Wi = 2.9$ for flow between rigid surfaces, (b) instability patterns disappeared for flow on 4 mm (2% cross-linker) PDMS gel ($\Gamma/Wi = \eta_0/(G'\lambda) = 5.8 \times 10^{-4}$), and (c) presence of instability pattern on hard (10% cross-linker) PDMS gel ($\Gamma/Wi = \eta_0/(G'\lambda) = 1.6 \times 10^{-7}$). Aspect ratio of the fluid = 0.075.

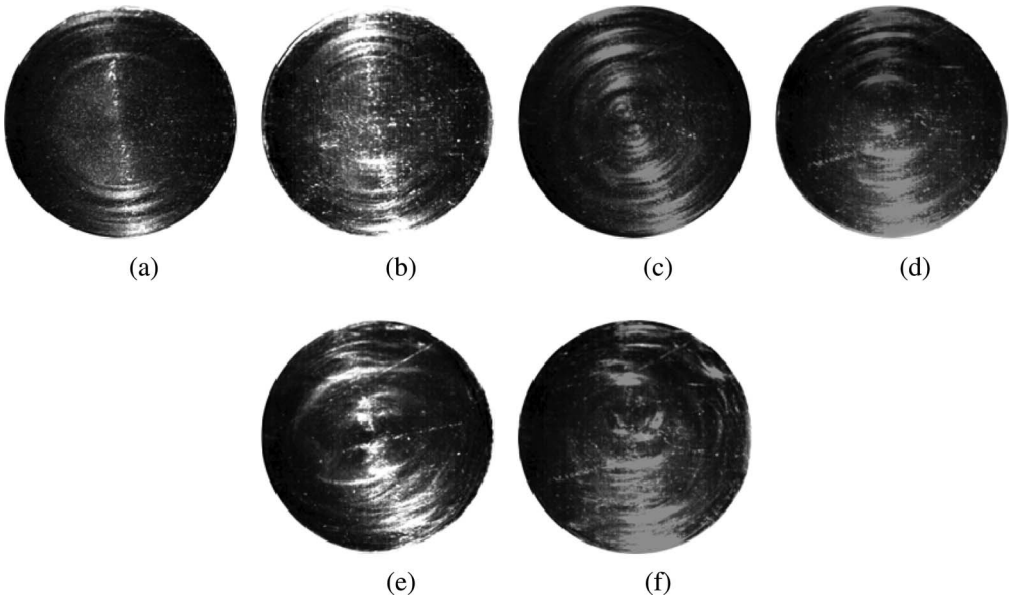

FIG. 16. Representative snapshots of flow 300 ppm polymer solution (at 25 °C $M_w \sim 5 \times 10^6$ g mol^{-1}, $\lambda = 2.9$ s) for controlled shear rates of 4, 7 and 10 s^{-1} between rigid plates (panels (a), (c), (e)) and on the 2% cross-linker PDMS gel of thickness 4 mm ($\Gamma/Wi = \eta_0/(G'\lambda) = 5.8 \times 10^{-4}$; panels (b), (d), (f)). The figures show that at higher shear rates, the purely elastic instability appears in the flow over the gel, and the instability patterns are similar in both cases. The aspect ratio $d/R = 0.075$.

of the absence of elastic instability for flow over the soft gel. In marked contrast, at various values of higher shear rates (>4 s^{-1}; Figure 16), the rheological behavior and flow patterns are same for flow over both rigid surface and the soft (2% cross-linker) gel. This demonstrates that the suppression of instability in flow over the soft gel happens only at intermediate shear rates, while at higher shear rates, the destabilizing elastic stresses in the bulk of the flow dominate the dynamics. This also supports the mechanism proposed above based on the compression of the gel leading to lower effective shear rates in the fluid.

IV. DISCUSSION

In Figure 18, we plot the Weissenberg number required to initiate the purely elastic instability as a function of the softness of the gel, as measured by the non-dimensional group $\Gamma/Wi = \eta_0/G'\lambda$. The critical Wi for instability in flow past a rigid plate is the value of Wi at which there is an abrupt viscosity increase for the first time in the data. For flow past the soft (2% cross-linker) gel, the viscosity continues to shear thin, but at higher shear rates, the data for flow past the gel merge with that of rigid surfaces. We define the critical Wi for flow past a gel as the value for which the apparent viscosity curves for flow past gels and the rigid plate merge first at higher Wi. As shown by Figure 17, the critical Wi increases with increase in $\eta_0/G'\lambda$, or in other words, Wi increases as the gel becomes more softer.

From the above experiments, it is clear that the suppression of instability is due to the deformability of the gel. However, the non-dimensional parameter $\Gamma = \dot{\gamma}\eta_0/G'$ is at most of $O(10^{-2})$ in our experiments. This parameter is the ratio of viscous shear stresses in the fluid to the elastic shear stresses in the solid, and is a measure of shear deformability of the solid. Since $\Gamma \sim 10^{-2}$, this appears too low to explain the origin of instability suppression. Instead, it is possible that the bulk compression of the gel due to the first-normal stress difference in the fluid could play a role in the instability suppression. We now carry out a scaling-level analysis to demonstrate the role of gel compression. The compressive strain ϵ in the gel due to the first normal-stress difference is $\epsilon \sim T_{11}/K$. The first-normal stress difference in the polymer solution, within the Oldroyd-B model, is

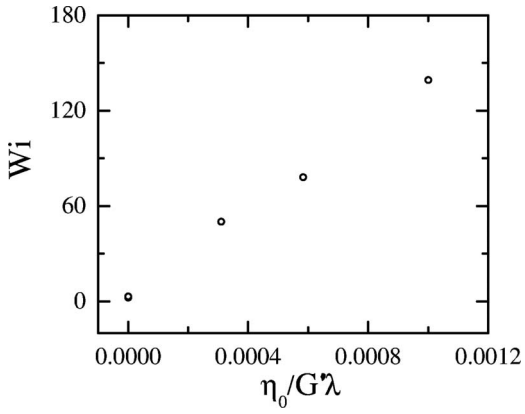

FIG. 17. Variation of the Weissenberg number required for instability with the non-dimensional elasticity parameter $\eta_0/(G'\lambda)$. The critical Wi required for destabilization increases with increase in $\eta_0/(G'\lambda)$, thereby showing that the more softer the gel, the higher the Wi for destabilization.

$T_{11} = 2\eta_0\dot{\gamma}^2\lambda$. For the 2% cross-linker gel, using typical values for viscosity and relaxation time η_0 = 1 Pa s, $\dot{\gamma} = 10\text{s}^{-1}$, $\lambda = 5$ s, we obtain $T_{11} \sim 10^3$ Pa. The compressional strain in the gel (using K = 2000 Pa) is given by $T_{11}/K \sim 0.5$. The original thickness of the gel is 2 mm, and thus, the change in the thickness of the gel is $0.5 \times 2 = 1$ mm. This means that the fluid thickness has increased effectively by 1 mm, so the actual fluid thickness is 2 mm. The shear rate in the fluid is given by $\Omega R/d$, and is effectively reduced by a factor of half due to the increased fluid thickness. Since the effective shear rate in the flow is lower, the first-normal stress difference is also effectively lower, and the purely elastic instability driven by the first-normal stress difference is delayed. When the effective shear rate reaches the value corresponding to that required for the purely elastic instability, the flow becomes unstable. Hence, it appears likely that the compression of the gel due to first-normal stress difference could be the reason behind the delay in purely elastic instability.

For the 5% cross-linker gel, however, the bulk modulus is very high (of $O(10^6)$ Pa), and hence the compressional strain due to the first normal stress difference in the fluid is $O(10^{-3})$ which is three orders of magnitude smaller than that for the 2% cross-linker gel. Hence, the gel does not have much effect on the delay in the instability, and the results are very similar to those for flow past a rigid surface. However, we measured the bulk (compression) modulus only in the linear stress regime, and it is highly possible that at finite normal stresses, the value will be different from that used in the above calculation. In addition, we could measure the bulk modulus when there is pure normal compression of the gel. In the flow experiments past the gel, the gel is compressed and sheared simultaneously, and in principle, when the shear strain in the gel is large, the compression modulus could become a function of the shear strain. However, this cannot be measured using the rheometer, and could have a bearing on the eventual destabilization of the flow at higher shear rates. Thus, while the previous works[16,19] have demonstrated the role of the shear modulus in destabilizing the flow of Newtonian fluids past a gel, the present work suggests the stabilizing role of the compression modulus in the torsional flow of polymer solutions.

V. CONCLUSION

We have carried out a comprehensive experimental study to understand the effect of a soft gel on the torsional flow of a polymer solution in the parallel-plate geometry of a rheometer. Torsional flows of polymer solutions typically undergo purely elastic instabilities driven by the first normal stress difference in the flow with increase in shear rate, which eventually results in an elastic turbulent state. The purely elastic instability in the torsional flow between rigid surfaces is characterized by an apparent shear thickening, marked hysteresis, and large temporal stress fluctuations after the onset of the instability. Further, distinct secondary flow patterns appear once the instability sets in. In this paper, we have shown that when the polymer solution flows past a soft gel, the elastic

instability is suppressed for intermediate values of shear rate. We find that the polymer solution continues to shear thin when it flows past a gel, in contrast to a rigid surface, up to a shear rate of 10 s^{-1}. The suppression of the purely elastic instability could be explained based on the finite bulk (compression) modulus of the gel. We postulate that the first-normal stress difference exerted by the fluid compresses the gel, leading to an effective increase in the fluid thickness, and hence a decrease in the effective shear rate of the flow. However, once the effective shear rate in the flow reaches the value required for the purely elastic instability, the behavior of the apparent viscosity is similar for both flow between rigid plates and flow over a gel. This explains why the instability suppression is not seen in the flow of polymeric fluids past gels (5% and 10% cross-linker) with $K \sim 1$ MPa. We have carried out flow visualization experiments to show that the secondary flow patterns that form after the instability disappear in the presence of the gel. Further, the flow over gel also does not exhibit hysteresis in contrast to flow between rigid surfaces. Previous studies on the torsional flow of Newtonian fluids over a soft gel have shown that the gel deformability (due to low shear modulus values) destabilizes the flow.[16,19] Our results show that, in marked contrast, at intermediate values of shear rate, the finite values of the bulk modulus of the gel has a stabilizing effect on the purely elastic instability in torsional flow of polymeric liquids.

The results of our study are also relevant to the understanding of the dynamics of the shear-banded states[13–15] in worm-like micellar solutions. In such systems, it is often found that upon increase in shear rate, there is a structural transition to a gel-like phase and a fluid-like phase co-existing in the flow. Our experimental system explicitly mimics this scenario, by using a soft gel and a polymer solution. It has been argued in previous studies that in such systems the fluid-"gel" interface can become unstable, much akin to the instability of a Newtonian fluid flow past a soft gel,[17,19] and experimental data for the apparent viscosity have been interpreted with the gel-instability hypothesis. However, by explicitly carrying out experiments of flow of polymeric liquids over a soft gel in a rotating disc geometry, we show, in contrast, that the deformability of the gel could have a stabilizing effect on the first-normal-stress-driven instability in polymer solutions. Our results suggest that the notion that deformability of the gel tends to destabilize the flow is perhaps not always valid for polymer solutions, and therefore indicate that more detailed experimental investigations are needed in worm-like micellar solutions in order to better understand the dynamics of the phase-separated shear-banded state.

ACKNOWLEDGMENTS

We thank Dr. Animangsu Ghatak for suggestions in the preparation of the gel, Professor V. Kumaran and Dr. Ashish Lele for suggestions in carrying out the experiments, and Professor Victor Steinberg and Professor Alexander Groisman for suggestions in determining longest relaxation time of polymer. We thank the anonymous referees for the suggestion regarding the mechanism of the instability. The Board of Research in Nuclear Sciences (BRNS), Department of Atomic Energy (DAE), Government of India (Grant No. 2007/36/48-BRNS) is acknowledged for financial support of this work.

APPENDIX: TORSIONAL FLOW OF POLYMER SOLUTIONS BETWEEN RIGID SURFACES

In this appendix, we describe experimental observations for flow of polymer solution between rigid surfaces in various rheometer configurations to fully characterize the instability seen at shear rates of $O(1)s^{-1}$ at temperatures near 25 °C. We first carried out experiments for flow between rigid plates with conditions (viz., polymer concentrations and temperature) similar to Schiamberg *et al.*[10] in order to benchmark our experimental results. We used the 400 ppm polyacrylamide solution ($M_w \sim 5 \times 10^6$ g mol^{-1}, $\lambda = 12$ s) in a solvent of 65.9% saccharose and 1% NaCl in water in the cone-and-plate (radius: 30 mm, cone angle: 0.035 radians) configuration. The experiment is carried out at 19 °C in the rate-controlled mode, and the observed viscosity is plotted as a function of Wi (non-dimensional shear rate) in Figure 18. The apparent viscosity shows a significant increase at a critical shear rate of 13 s^{-1}. The observed critical shear rate in our experiments is little more compared to the value of 8 s^{-1} of Ref. 10, presumably due to the fact that in our set up, the top

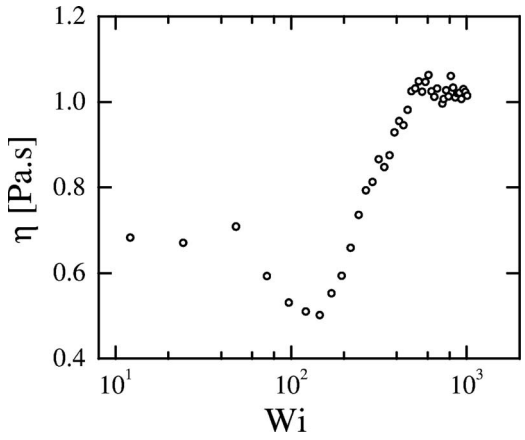

FIG. 18. Validation of purely elastic instability observed in our study conducted at conditions similar to those of Ref. 10: Data showing the variation of apparent viscosity with Wi. The experiment was conducted in the shear rate controlled mode with 400 ppm polyacrylamide solution ($M_w \sim 5 \times 10^6$ g mol^{-1}, $\lambda = 12$ s) in 65.9% saccharose and 1%NaCl in water (temperature: 19 ° C) in the cone-and-plate configuration of the rheometer (60 mm dia and cone angle 0.035 radians). The error bars for the apparent viscosity in the viscometric regime is at most 5%, while the spread of the data in the unstable regime has standard deviation of at most 25%.

plate radius is more and cone angle is less compared to the values of Ref. 10. This increase in critical shear rate is in agreement with the experimental observations of Magda and Larson[3] The zero-shear viscosity and solvent viscosity are close to the values reported in Ref. 10. Interestingly, our experiments also suggest the presence of a small viscosity "bump" at 3 s^{-1} (Figure 18), and this rheological feature was not reported by earlier works at 19 °C. However, Schiamberg *et al.*[10] do report an increase in the first normal stress difference (measured using an ARES rheometer) at a shear rate of 3 s^{-1}, which could be interpreted as a signature of the instability of the flow. However, we were unable to measure the normal stress developed at the onset of instability with our AR 1000N rheometer, since the normal force sensor at bottom plate does not have the capacity to sense small amounts of normal force in any configuration of the rheometer.

To examine whether this increase in apparent viscosity occurs for other geometries as well, we carried out experiments in parallel plate and concentric cylinder configurations of the rheometer, as discussed in the main text (Figure 6). Our results show that the increase in apparent viscosity occurs at about 3 and 1 s^{-1} for cone-and-plate and parallel-plate geometries, respectively, but not in the concentric cylinder geometry. It must be noted that the earlier experiments[9,10] were carried out at temperatures below 20 °C. However, the ambient conditions in our laboratory do not allow us to maintain the polymer solution below 25 °C. Hence, most of our experiments are conducted at the ambient temperature (25 ± 2 °C) maintained using air-conditioners. While the rheometer has a built-in temperature control with a Peltier plate where we could maintain the temperature below 20 °C, we could not keep the fluid thickness larger than 2 mm in the standard rheometer arrangement,[3] as the surface tension at the rim was insufficient to hold the fluid. In addition, when we study the effect of the soft solid on the instability, the bottom plate of the rheometer must be coated with a layer of the gel. It was found difficult to maintain the fluid and the gel at desired temperatures using the Peltier plate of the rheometer.

To examine whether the appearance of instability depends on the mode of operation of the instrument, we carried out experiments in both stress and rate-controlled mode, and the results are reported in Figure 19. As mentioned in Sec. II, we use a petri dish instead of the bottom plate which enables us to use higher aspect ratios than allowed by the rheometer configuration, and the transparent nature of the petri-dish also aids in the visualization of the flow. In Figure 19, we plot the apparent viscosity obtained from parallel plate and concentric cylinder configurations versus Wi (in the controlled-stress mode) for the 492 ppm polyacrylamide solution ($M_w = 18 \times 10^6$ g mol^{-1}, $\lambda = 18$ s). In the stress-controlled experiment, the Wi is calculated by estimating the shear rate as

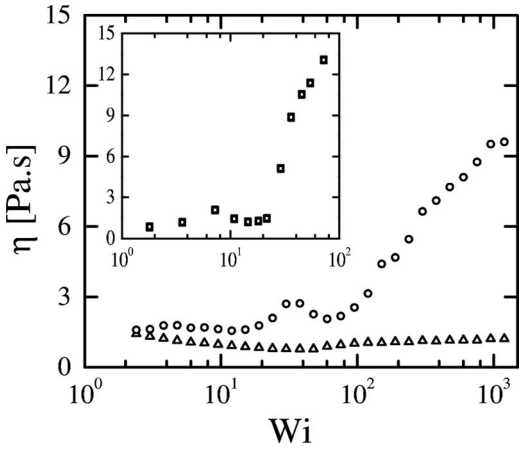

FIG. 19. Apparent viscosity of parallel plate (open circles) and concentric cylinder (open triangle) data versus Wi for the 492 ppm polyacrylamide ($M_w = 18 \times 10^6$ g mol^{-1}) solution in 65.9% of saccharose, and 1% NaCl in water, with $\lambda = 18$ s. The measurement was carried out with parallel plate (aspect ratio = 0.204) and concentric cylinder (fluid thickness 1 mm and inner dia 28 mm) geometries at 25 °C. The experiments were conducted in the stress-controlled mode. The inset shows the (time-average) ratio of viscosities from parallel plate and concentric cylinder geometries versus Wi done using the rate-controlled mode for the same system. The error bars for the apparent viscosity in the viscometric regime is at most 5%, while the spread of the data in the unstable regime has standard deviation of at most 25%.

τ/η_0, and this is multiplied by relaxation time λ. The inset shows the viscosity ratio (of the parallel plate and concentric cylinder data) as a function of Wi in the rate-controlled mode. The elastic instability begins at a critical shear rate of 0.2 s^{-1} for both stress and strain rate controlled mode. Thus, both stress- and rate- control modes exhibit similar behavior. We also find that there is no appreciable viscous dissipation of flow, and hence no substantial increase in temperature of the solution was observed.[10]

In Figure 20, we show the apparent viscosity as a function of Wi for 492 ppm ($M_w = 18 \times 10^6$ g mol^{-1}, $\lambda = 18$ s) polyacrylamide solution. The flow pattern is visualized over a range of shear stress values from 0.092 to 58 Pa (the corresponding Weissenberg number ranges from 1.1 to 696, and Reynolds number of the flow lies between 0.0002 and 0.11). Initially, the shear rate is constant

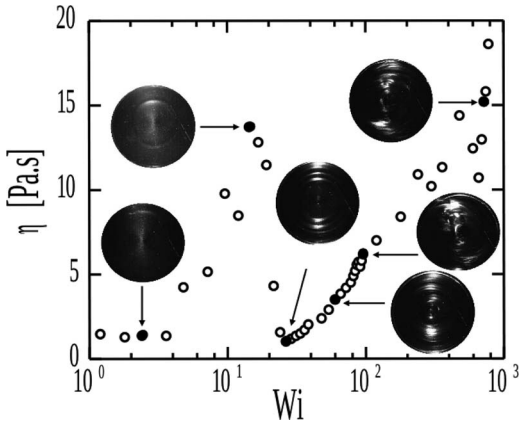

FIG. 20. Apparent viscosity as a function of Wi (in the stress-controlled mode) at 25 ° C for the 492 ppm polyacrylamide solution ($M_w = 18 \times 10^6$ g mol^{-1}) dissolved with 65.9% saccharose and 1% NaCl in water ($\lambda = 18$ s). The aspect ratio of the system in parallel plate-arrangement is $d/R = 0.1275$. The snapshots show the progression of the instability patterns associated with the rheological signatures. The error bars for the apparent viscosity in the viscometric regime is at most 5%, while the spread of the data in the unstable regime has standard deviation of at most 25%.

at a given stress value; the flow is uniform and azimuthal in nature. Following Ref. 10, we correlated the change in the shear rate for a stress step with corresponding changes in flow patterns and labelled the instability patterns for different values of τ or Wi. With increase in stress in small steps, the flow shows shear thickening behavior which begins at $\tau = 0.4$ Pa, and a circular ("concentric ring") pattern begins to form near the edge of the top plate and shear rate fluctuates with time. The subsequent increase in stress shows more pronounced shear rate variation with time and the diameter of the ring patterns gradually decreases, which resides in between the center and the edge of top plate. With further increase in the stress, the pattern collapses, and additional ring ("competing spiral") patterns are formed between the center and edge of the plate, which finally leads to spiral patterns accompanied by a gradual decrease in shear rate with time. A decrease in shear rate is associated with the disappearance of spiral pattern cycle, and this mode was referred to as "multi-spiral chaotic mode." When the stress is increased, the spirals disappear and reappear ("spiral bursting") at locations other than the center of the top parallel plate. At higher stress values, the flow is comprised of random appearance of spirals and their bursting, which is accompanied by large irregular fluctuations ("elastic turbulence") in shear rate with time. The entire progression of the various instability modes observed in our work is similar to the one reported in Ref. 10. In addition to the above experimental characterization, the appearance of different instability modes in flow between parallel plates was also studied using the other (200 ppm) polyacrylamide solution. The flow pattern was visualized over a range of fixed shear stress values from 0.092 to 60 Pa. We find (data not shown) an identical progression (similar to Figure 20) of instability modes with increase in shear stress in polymer solutions with 492 ppm.

When the flow was visualized at the shear rate (around 1 s^{-1}) at which there is a viscosity increase in our experiments, we found flow structures similar to what Schiamberg *et al.*[10] refer to as the "concentric ring" mode, as can be seen in Figure 20. It is interesting to note that the concentric ring mode was also visualized by Schiamberg *et al.*[10] at 19 °C at about 1 s^{-1}, but their rheological data do not exhibit a viscosity increase at this shear rate. In contrast, our experiments at 25 °C show a viscosity increase as well as the concentric ring flow structure at the shear rate of 1 s^{-1}. To better understand the reason for the prominent rheological signature of the instability at 1 s^{-1} for 25 °C, we performed steady-state experiments at different temperatures for the 300 ppm polyacrylamide with 63% saccharose in water using a cone-and-plate geometry. The cone-and-plate geometry facilitates uniform flow azimuthally with better temperature control between the plates. In Figure 21, we show the apparent viscosity as a function of shear stress (inset: as a

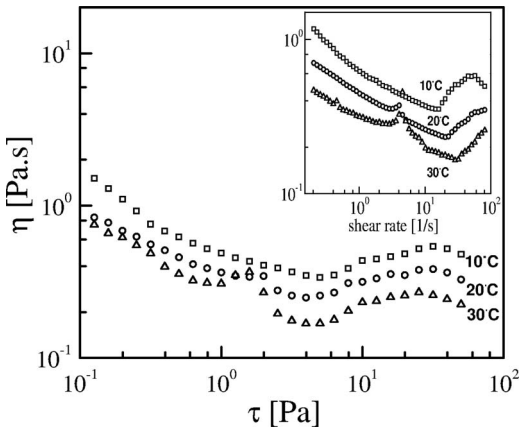

FIG. 21. Apparent viscosity as a function of shear stress (inset: shear rate) for the 300 ppm polyacrylamide solution with 63% saccharose in water. The experiment was conducted in the cone-and-plate geometry at three different temperatures (10, 20, and 30 °C). The shear rates and shear stresses are not nodimensionalized as the relaxation time is different for the three solutions. The relaxation time for the polymer solution at 25 ° C is 4.3 s. The figure demonstrates that the purely elastic instability mode found in this study appears at higher temperatures of 20 °C and 30 °C, but not at 10 °C. The error bars for the apparent viscosity in the viscometric regime is at most 5%, while the spread of the data in the unstable regime has standard deviation of at most 25%.

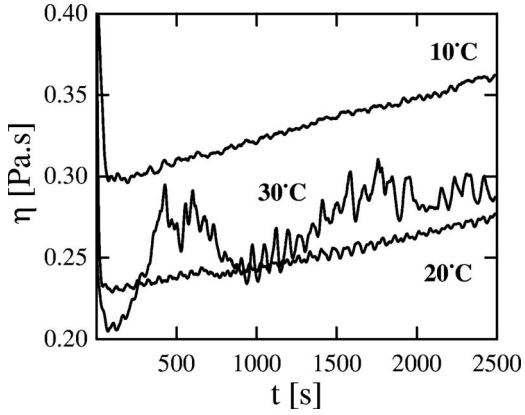

FIG. 22. Time-dependent viscosity variation for the 300 ppm polyacrylamide solution with 63% saccharose in water ($M_w \sim 5 \times 10^6$ g mol^{-1}, $\lambda = 4.3$ s at 25 °C) at a constant shear stress of 1.3 Pa, and at different temperatures (10, 20, and 30 °C). The experiment was carried out in the cone-and-plate geometry (60 mm dia and cone angle 0.035 radians). The shear stress value of 1.3 Pa is chosen such that this is above the critical shear stress required for the purely elastic instability at 30 °C. The data show minimal fluctuations at 10 °C, while the fluctuations are highly predominant at 30 °C indicating that the flow is unstable at this temperature, while it is stable at lower temperatures.

TABLE IV. Critical shear rate for polymer solutions in the parallel-plate geometry (aspect ratio: 0.204).

Polymer concentration [ppm]	M_w of polymer [g/mol]	Saccharose concentration %	Critical shear rate [1/s]	λ [s]
200	18×10^6	65.9	3.54	6
350	18×10^6	65.9	0.67	7.4
492	18×10^6	65.9	0.2	18

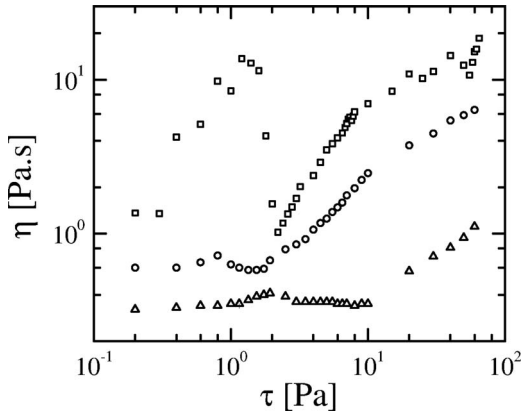

FIG. 23. Onset of purely elastic instability as a function of polymer concentration in flow between rigid parallel plates: Apparent viscosity of the 200 [triangle], 350 [circle], and 492 [square] ppm polyacrylamide ($M_w = 18 \times 10^6$ g mol^{-1}) solution with 65.9% saccharose and 1% NaCl in water. The experiment was carried out in the stress-controlled mode of the parallel-plate geometry (aspect ratio = 0.204) at temperature 25 ± 2 °C. The data show that the critical shear rate for the onset of viscosity increase (a signature of the instability) decreases with increase in polymer concentration, and therefore with relaxation time of the solution, in agreement with the expectation for the purely elastic instability. The relaxation times are respectively 6, 7.4, and 18 s for the 199, 350, and 492 ppm solutions. The error bars for the apparent viscosity in the viscometric regime is at most 5%, while the spread of the data in the unstable regime has standard deviation of at most 25%.

function of shear rate) at three different temperatures viz., 10, 20 and 30 °C (also see Ref. 24 for a discussion on the effect of temperature). The decrease in viscosity (at a given shear stress or shear rate) with increase in temperature is attributed to the decrease in solvent viscosity with increase in temperature. At 10 °C, the viscosity shear thins up to a shear rate of 20 s^{-1}, while at higher temperatures, there is an abrupt increase of viscosity at a shear rate of around 2 s^{-1}. To ascertain that this abrupt increase in viscosity is indeed a flow phenomenon, and not due to any artifacts such as polymer degradation,[4] we have verified that the same behavior is observed when the experiment was repeated on the same polymer solution at 20 and 30 °C. We further recorded the variation of apparent viscosity with time at a fixed shear stress (shown in Figure 22), and this shows that at 10 °C, there are no significant fluctuations in the apparent viscosity signal for about 1 h, while at 20 °C, the magnitude of the viscosity fluctuations increase, while the fluctuations are most prominent at 30 °C.

Finally, we also carried out experiments at different concentrations at a given temperature, and the key results are summarized in Table IV. The corresponding data for apparent viscosity are shown in Figure 23 (stress-controlled mode, parallel-plate geometry). These data show that at a fixed temperature, the shear rate at which the viscosity bump appears decreases with increase in concentration of the polymer. This is in qualitative agreement with earlier experimental predictions,[3] since at higher concentrations, the relaxation time of the polymer solution will increase, and consequently the actual shear rate at which the elastic instability appears will decrease. Therefore, the decrease in shear rate (at which the flow becomes unstable) with increase in polymer concentration is in agreement with earlier works, and substantiates the conclusion that viscosity "bump" seen at 1 s^{-1} is indeed a signature of the purely elastic instability.

[1] N. Phan-Thien, "Coaxial-disc flow of an Oldroyd-B fluid: Exact solution and stability," J. Non-Newtonian Fluid Mech. **13**, 325 (1983).
[2] N. Phan-Thien, "Cone-and-plate flow of the Oldroyd-B fluid is unstable," J. Non-Newtonian Fluid Mech. **17**, 37 (1985).
[3] J. Magda and R. G. Larson, "A transition occurring in ideal elastic liquids during shear flow," J. Non-Newtonian Fluid Mech. **30**, 1 (1988).
[4] G. McKinley, J. Byars, R. Brown, and R. C. Armstrong, "Observations on the elastic instability in cone-and-plate and parallel-plate flow of a polyisobutylene Boger fluid," J. Non-Newtonian Fluid Mech. **40**, 201 (1991).
[5] D. O. Olagunju and L. P. Cook, "Secondary flows in cone-and-plate flow of an Oldroyd-B fluid," J. Non-Newtonian Fluid Mech. **46**, 29 (1993).
[6] J. A. Byars, A. Oztekin, R. A. Brown, and G. H. McKinley, "Spiral instabilities in the flow of highly elastic fluids between rotating parallel disc," J. Fluid Mech. **271**, 173 (1994).
[7] E. S. G. Shaqfeh, "Purely elastic instabilities in viscometric flows," Annu. Rev. Fluid Mech. **28**, 129 (1996).
[8] A. Groisman and V. Steinberg, "Elastic turbulence in a polymer solution flow," Nature (London) **405**, 53 (2000).
[9] A. Groisman and V. Steinberg, "Elastic turbulence in curvilinear flows of polymer solution," New J. Phys. **6**, 29 (2004).
[10] B. A. Schiamberg, I. T. Shereda, H. Hu, and R. G. Larson, "Transitional pathway to elastic turbulence in torsional, parallel-plate flow of polymer solution," J. Fluid Mech. **554**, 191 (2006).
[11] T. M. Squires and S. R. Quake, "Microfluidics: Fluid physics at the nanoliter scale," Rev. Mod. Phys. **77**, 977 (2005).
[12] J. C. McDonald and G. M. Whitesides, "Poly(dimethylsiloxane) as a material for fabricating microfluidic devices," Acc. Chem. Res. **35**, 491 (2002).
[13] M. Vasudevan, A. Shen, B. Khomami, and R. Sureshkumar, "Self-similar shear thickening behavior in CTAB/NaSal surfactant solutions," J. Rheol. **52**, 527 (2008).
[14] M. A. Fardin *et al.*, "Elastic turbulence in shear banding wormlike micelles," Phys. Rev. Lett. **104**, 178303 (2010).
[15] P. Nghe, S. M. Fielding, P. Tabeling, and A. Ajdari, "Interfacially driven instability in the microchannel flow of a shear-banding fluid," Phys. Rev. Lett. **104**, 248303 (2010).
[16] V. Kumaran and R. Muralikrishnan, "Spontaneous growth of fluctuations in the viscous flow of a fluid past a soft interface," Phys. Rev. Lett. **84**, 3310 (2000).
[17] R. Muralikrishnan and V. Kumaran, "Experimental study of the instability of viscous flow past a flexible surface," Phys. Fluids **14**, 775 (2002).
[18] V. Kumaran, G. H. Fredrickson, and P. Pincus, "Flow induced instability of the interface between a fluid and a gel at low Reynolds number," J. Phys. II France **4**, 893 (1994).
[19] M. D. Eggert and S. Kumar, "Observations of instability, hysterisis, and oscillation in low-Reynolds number flow past polymer gels," J. Colloid Interface Sci. **278**, 234 (2004).
[20] M. K. S. Verma and V. Kumaran, "A dynamical instability due to fluidwall coupling lowers the transition Reynolds number in the flow through a flexible tube," J. Fluid Mech. **705**, 322 (2012).

[21] V. Shankar and S. Kumar, "Instability of viscoelastic plane Couette flow past a deformable wall," J. Non-Newtonian Fluid Mech. **116**, 371 (2004).
[22] P. Choskshi and V. Kumaran, "Stability of the flow of a viscoelastic fluid past a deformable surface in the low Reynolds number limit," Phys. Fluids **19**, 104103 (2007).
[23] J. D. Ferry, *Viscoelastic Properties of Polymers* (John Wiley, New York, 1980).
[24] J. P. Rothstein and G. H. McKinley, "Non-isothermal modification of purely elastic flow instabilities in torsional flows of polymeric fluids," Phys. Fluids **13**, 382 (2001).